

Structural optimization of oxaprozin for selective inverse Nurr1 agonism

Sabine Willems^{1*}, Romy Busch¹, Felix Nawa¹, Marco Ballarotto^{1,3}, Felix F. Lillich^{2,4}, Till Kasch¹, Úrsula López-García¹, Julian A. Marschner¹, Lorena A. Rüger², Beatrice Renelt², Julia Ohrndorf², Silvia Arifi², Daniel Zaienne², Ewgenij Proschak^{2,4}, Jörg Pabel¹, Daniel Merk^{1,2*}

¹ Department of Pharmacy, Ludwig-Maximilians-Universität München, 81377 Munich, Germany

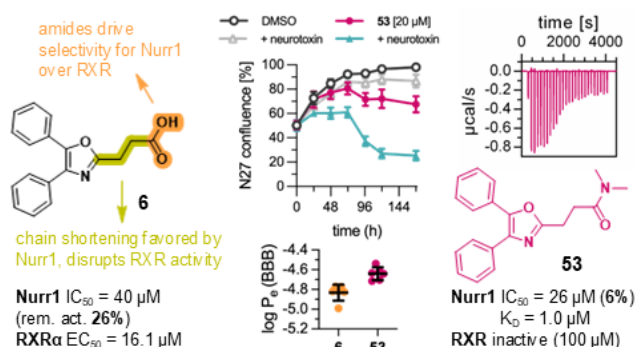
² Institute of Pharmaceutical Chemistry, Goethe University Frankfurt, 60438 Frankfurt, Germany

³ Department of Pharmaceutical Sciences, Università degli Studi di Perugia, 06123 Perugia, Italy

⁴ Fraunhofer Institute for Translational Medicine and Pharmacology ITMP, 60596 Frankfurt, Germany

Keywords: nuclear receptor related-1, transcription factor, NR4A2, neurodegeneration, Alzheimer's Disease, Parkinson's Disease

Abstract: Nuclear receptor related 1 (Nurr1, NR4A2) is a ligand-sensing transcription factor with neuroprotective and anti-inflammatory roles widely distributed in the CNS. Pharmacological Nurr1 modulation is considered a promising experimental strategy in Parkinson's and Alzheimer's disease but target validation is incomplete. While significant progress has been made in Nurr1 agonist development, inverse agonists blocking the receptor's constitutive activity are lacking. Here we report comprehensive structure-activity relationship elucidation of oxaprozin which acts as moderately potent and non-selective inverse Nurr1 agonist and RXR agonist. We identified structural determinants selectively driving RXR agonism or inverse Nurr1 agonism of the scaffold enabling the development of selective inverse Nurr1 agonists with enhanced potency and strong efficacy.

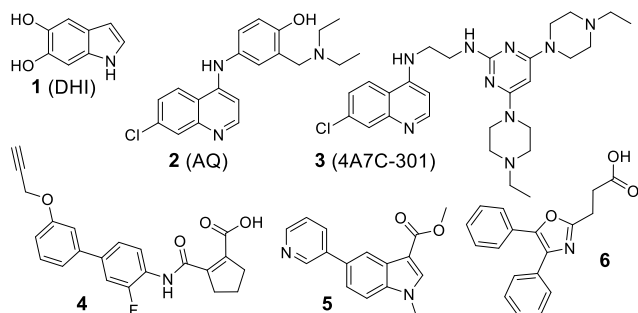


Introduction

The ligand-activated transcription factor nuclear receptor-related 1 (Nurr1, NR4A2)¹ emerges as a highly promising target for the treatment of Parkinson's Disease (PD) and other neurodegenerative disorders². It is a member of the nerve growth factor IB-like receptor family (NR4A)³ and highly expressed in the CNS, particularly in dopaminergic neurons⁴. Altered Nurr1 expression levels in patients with PD⁵, Alzheimer's Disease (AD)^{6,7} and multiple sclerosis (MS)⁸ as well as in well-established rodent models of neurodegenerative diseases (5XFAD⁶ and MPTP⁵) provide convincing evidence for a key role of Nurr1 in neurodegeneration. Moreover, heterozygous Nurr1 knockout in mice accelerated experimental autoimmune encephalomyelitis (EAE)⁹ and mice with Nurr1 knockout in dopaminergic neurons revealed a PD-like phenotype⁴. These observations suggest great therapeutic potential of pharmacological Nurr1 modulation in neurodegenerative diseases^{6-8,10} prompting the search for Nurr1 modulating small molecules.

The collection of available Nurr1 activators discovered and developed to date comprises the dopamine metabolite 5,6-dihydroxyindole (DHI, **1**)¹¹ and natural fatty acid metabolites^{12,13}, the anti-malarial amodiaquine (AQ, **2**)^{14,15}, the AQ-descendent 4A7C-301 (**3**)¹⁶, AQ-derived fragments¹⁷ and analogues of DHI¹⁸ (Chart 1). Furthermore, we have recently developed the high-affinity Nurr1 agonist **4**¹⁹ and mimetics derived by *de novo* design²⁰ as next-generation chemical tools. These structurally diverse scaffolds provide a basis for the development of potent Nurr1 agonists.

Chart 1. Selected Nurr1 ligands



However, Nurr1 has remarkable constitutive transcriptional inducer activity¹ and, therefore, can be modulated in a bidirectional fashion. While Nurr1 agonists have been established as chemical tools^{16,21}, Nurr1 inhibition with small molecules is poorly explored. Especially for nuclear receptors with high intrinsic - ligand independent - activity like the NR4A and NR1F (retinoic acid receptor-related orphan receptors (RORs)) subfamilies, blocking baseline activity with inverse agonists is of interest for biological studies and, potentially, therapeutic purposes. While beneficial effects of inverse agonists have been demonstrated for ROR γ in the context of autoimmune diseases^{22,23}, therapeutic potential of inhibiting Nurr1 activity remains elusive and chemical tools to explore this field are needed. We have developed a first intermediately potent inverse Nurr1 agonist (**5**) from a fragment screening hit²⁴ and discovered a few non-steroidal anti-inflammatory drugs (NSAIDs) including oxaprozin (**6**)²⁵ as direct inhibitors of Nurr1 activity. Importantly, **5** and analogues comprised preference for blocking Nurr1 monomer activity²⁴ while **6** diminished the activity of Nurr1 as monomer, homodimer and heterodimer²⁵. Together, the chemotypes of **5** and **6** would hence form an attractive pair of tools to study biological effects of pharmacological Nurr1 blockade potentially discriminating monomer and dimer mediated effects. However, oxaprozin (**6**) is a weak inverse Nurr1 agonist (IC₅₀ 40 μ M) and additionally modulates the retinoid X receptor, another member of the nuclear receptor family and the heterodimer partner of Nurr1, preventing its use as an *in vitro* chemical tool.

To overcome these limitations and to provide selective oxaprozin-derived inverse Nurr1 agonists we have systematically studied the structure activity relationship (SAR) of the scaffold as Nurr1 modulator. We succeeded in tuning potency and selectivity of oxaprozin derivatives and obtained to our knowledge the most advanced inverse Nurr1 agonists available to date.

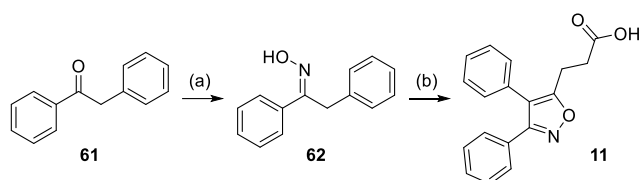
Results & Discussion

Chemistry

Oxaprozin derivatives **8**, **12–23**, **25–27**, **29–32**, **36–41**, and **51** were available from our previous studies^{26,27}, derivatives **6**, **7**, **9**, **10**, and **52–54** were commercially available, and compounds **11**, **24**, **28**, **33–35**, **42–50**, and **55–60** were prepared according to Schemes 1–6.

Synthesis of isoxazole derivative **11** followed a published two-step procedure²⁸ (Scheme 1). For this, phenylbenzylketone **61** was reacted with hydroxylamine to the corresponding oxime **62**, which was then cyclized with succinic anhydride (**63**) in the presence of *n*BuLi and subsequent dehydration with sulfuric acid to obtain isoxazole **11** in good yield.

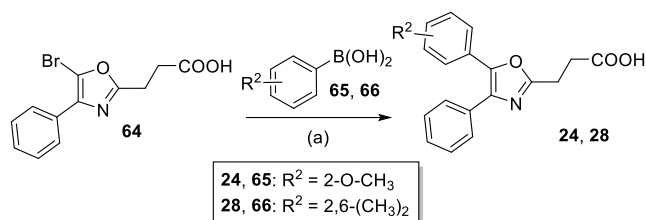
Scheme 1. Synthesis of **11**.^a



^a Reagents & Conditions: (a) hydroxylamine hydrochloride, KOH, EtOH, 30 min, r.t., then **61**, toluene, reflux, 16 h, 53%; (b) *n*BuLi, succinic anhydride (**63**), THF, -20 °C (1 h) and r.t. (16 h), then conc. H₂SO₄, reflux, 2 h, 61%.

Derivatives **24** and **28** were accessible by Suzuki coupling of the aryl bromide precursor **64** with boronic acids **65** or **66** in moderate yields (Scheme 2). Preparation of **64** has been published previously²⁶.

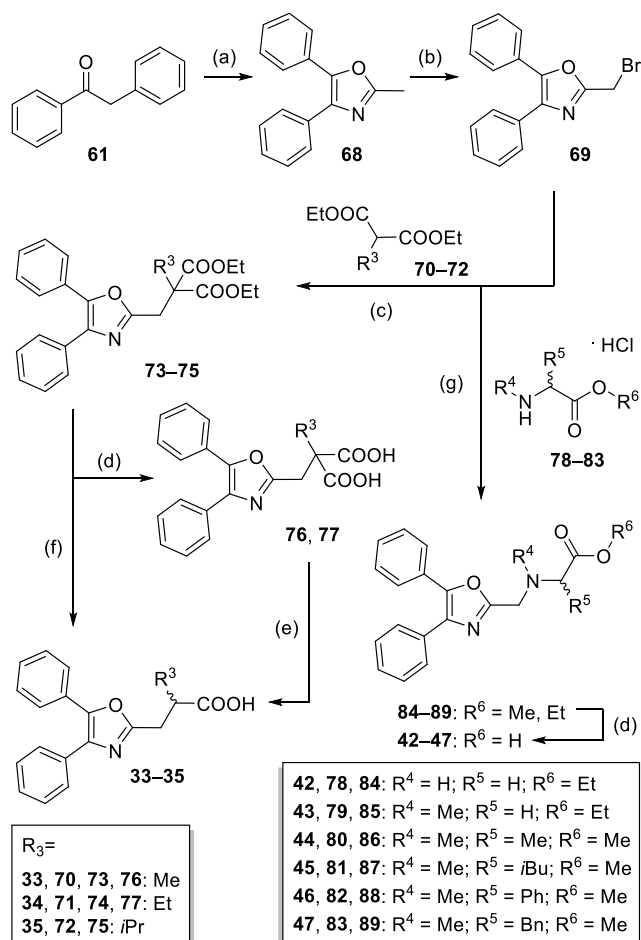
Scheme 2. Synthesis of 24, 28.^a



^a Reagents & Conditions: (a) Pd(Ph₃)₄, Na₂CO₃, dioxane/H₂O (4:1), 140 °C, 20 h, 39–42%.

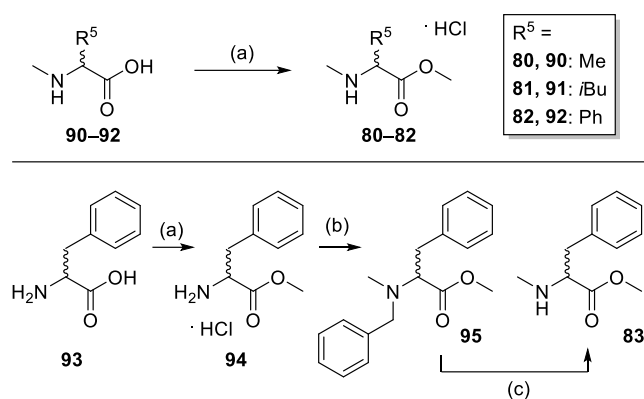
Synthesis of derivatives with a branched chain in α -position (**33–35**) as well as introduction of amino acid like motifs in the chain of **42–47** started from cyclization of phenylbenzylketone **61** with acetonitrile (**67**) in presence of iodine, TfOH and oxone to obtain the 2-methyloxazole **68** (Scheme 3)²⁹. Subsequent bromination³⁰ of **68** to **69** using NBS and AIBN followed by reaction with ethyl malonates **70–72** yielded **73–75**. Ester hydrolysis and decarboxylation yielded the free carboxylic acids **33–35**. Amino acids were introduced using the hydrochlorides of their respective esters (**78–83**) which were reacted under basic conditions with **69**. For this, the respective amino acids **90–92** were esterified to **80–82** using thionyl chloride in MeOH (Scheme 4). Building block **83** was prepared from DL- α -phenylalanine (**93**) in a three-step procedure. First, **93** was protected by esterification using thionyl chloride in MeOH to obtain **94**. Then, the amino group of **94** was benzylated and monomethylated by reductive amination according to a published procedure³¹ using benzaldehyde, NaBH₃CN and paraformaldehyde. The benzylic protecting group of **95** was then removed using NH₄HCO₂ and palladium on carbon in MeOH³² to obtain building block **83**.

Scheme 3. Synthesis of 33–35 and 42–47.^a



^a Reagents & Conditions: (a) ACN (**67**), I₂, oxone, TfOH, 70 °C, 6 h, 55%; (b) NBS, AIBN, CCl₄, 70 °C, 4 h, 49%; (c) NaH, THF, r.t.–50 °C, 16–22 h, 68–97%; (d) KOH, H₂O, 50–90 °C, 20–24 h, 38–97%; (e) HCl, H₂O, 95–110 °C, 24 h, 66–67%; (f) KOH, EtOH, 90 °C, 20 h, 80%; (g) NaHCO₃, THF/H₂O, 0–10 °C, 4 h, then r.t.–50 °C, 26–70 h, 49–78% or NaHCO₃, MeCN, r.t., 96–168 h, 19–83%.

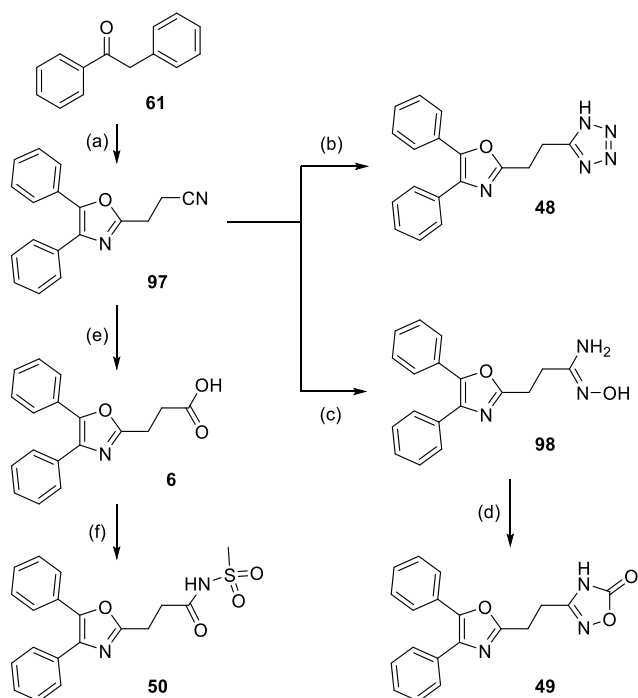
Scheme 4. Synthesis of building blocks 80–83.^a



^a Reagents & Conditions: (a) SOCl_2 , MeOH, 0 °C (2 h), then r.t. (16–144 h), 98%–quant.; (b) benzaldehyde, MeOH, r.t., 1 h, then NaBH_3CN , $(\text{CH}_2\text{O})_n$, r.t., 24 h, 38%; (c) NH_4HCO_2 , Pd/C, MeOH, reflux, 1 h, 15%.

Bioisosteres **48–50** of the carboxylic acid in **6** were prepared from phenylbenzylketone **61** which was cyclized with succinonitrile **96** to oxazole **97** in presence of iodine, TfOH and oxidant oxone according to a slightly modified procedure by Wu et al.³³ (Scheme 5). The 1*H*-tetrazole in **48** was obtained directly from the propanenitrile **97** via tin-catalyzed [3+2] cycloaddition using azidotri-*n*-butyltin(IV). Compound **49** was prepared over two steps from nitrile **97** according to a published procedure³⁴. First, the reaction of nitrile **97** with hydroxylamine provided hydroxyamidine **98** in good yield. The oxadiazolone **49** was then formed by refluxing **98** with CDI in THF. For compound **50**, hydrolysis of nitrile **97** under basic conditions provided oxaprozin (**6**)²⁹, which was subsequently coupled with methanesulfonamide in the presence of EDC and 4-DMAP³⁵.

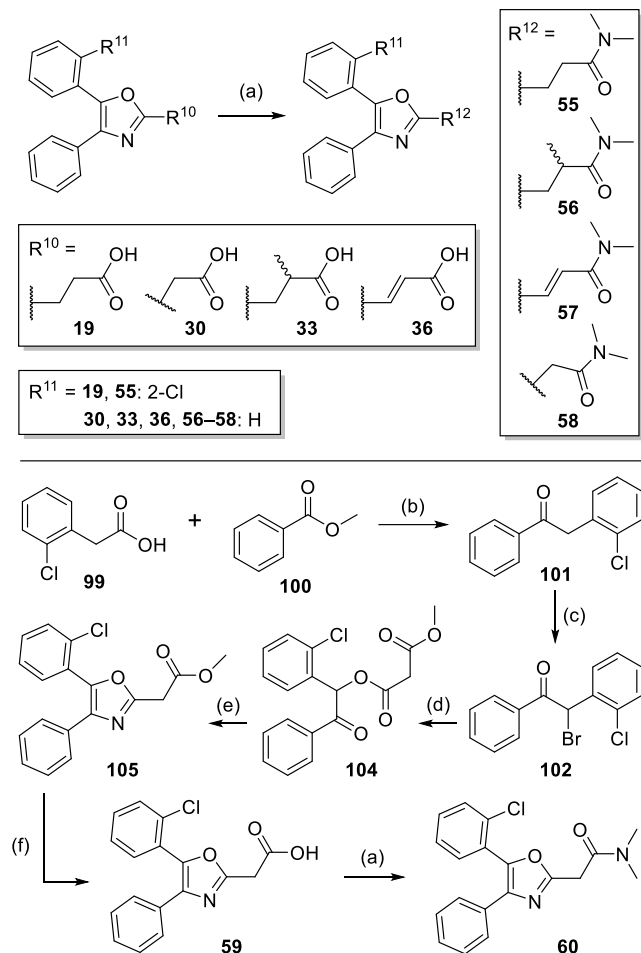
Scheme 5. Synthesis of 48–50.^a



^a Reagents & Conditions: (a) succinonitrile (**96**), oxone, I_2 , TfOH, 60 °C, 18 h, 49%; (b) azidotri-*n*-butyltin(IV), *p*-xylene, 150 °C, 18 h, 38%; (c) hydroxylamine, EtOH, 75 °C, 48 h, 82%; (d) CDI, THF, reflux, 16 h, 10%; (e) NaOH, 1,4-dioxane/ H_2O , r.t., 100 °C, 72 h, 45%; (f) $\text{NH}_2\text{SO}_2\text{Me}$, DMAP, EDC-HCl, DCM, r.t., 48 h, 71%.

The analogues **55–60** were prepared according to Scheme 6. The carboxylic acids of derivatives **19**, **30**, **33**, and **36** were coupled with dimethylamine hydrochloride in the presence of HATU and DIPEA to yield the respective dimethylamides **55–58**. Analogues **59** and **60** were prepared from 2-chlorophenylacetic acid **99**, which was coupled with methyl benzoate (**100**) in the presence of LiHMDS to obtain 2-chlorobenzyl phenyl ketone **101**. Bromination with NBS yielded the α -bromo ketone **102**, which was converted to the ester **104** through nucleophilic substitution by monomethyl malonic acid **103**. The ester **104** was then cyclized to oxazole **105** using NH_4OAc in acetic acid. Saponification of the methyl ester with LiOH yielded 2-oxazolylacetic acid **59**, which was subsequently coupled with dimethylamine hydrochloride in the presence of HATU and DIPEA to yield the dimethylacetamide **60**.

Scheme 6. Synthesis of 55–60.^a



^a Reagents & Conditions: (a) HATU, DIPEA, DMF, r.t., 30 min, then dimethylamino hydrochloride, r.t., overnight, 20–83%; (b), DMF, 0 °C, then LiHMDS, r.t., overnight, 85%; (c) NBS, *p*TsOH, DCM, reflux, overnight, 84%; (d) potassium monomethyl malonate (**103**), NEt_3 , acetone, reflux, overnight, 52%; (e) NH_4OAc , AcOH, 100 °C, overnight, 47%; (f) LiOH, MeOH/ H_2O , r.t., overnight, 19%.

Biological Evaluation

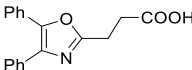
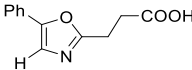
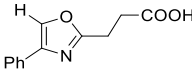
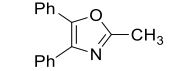
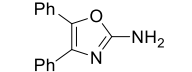
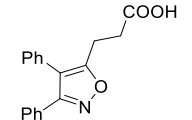
To optimize the oxaprozin scaffold for selective inverse Nurr1 agonism with no remaining activity on RXR, we have systematically studied its SAR for both transcription factors with analogues **7–60** and additionally considered SAR knowledge on structurally related RXR agonists from previous studies²⁶. Nurr1 and RXR α modulation by **6–60** were determined in uniform Gal4-hybrid reporter gene assays using the respective chimeric receptor to control a Gal4-responsive firefly luciferase as reporter gene. Constitutively expressed renilla luciferase (SV40 promoter) served to monitor transfection efficiency and test compound toxicity.

Structural Optimization

We commenced our SAR evaluation by probing the importance of the phenyl substituents and the carboxylic acid side chain of **6** (Table 1). While **6** blocked Nurr1 activity with an IC_{50} value of 40 μM and 26% remaining activity, removal of either phenyl substituent in 4- (**7**) or 5-position (**8**) was detrimental for inverse Nurr1 agonism. Removal of the polar side chain in methyl analogue **9**

markedly reduced and inverted activity on Nurr1 to weak agonism. Interestingly, the corresponding amine **10** retained inverse agonism. Changing the geometry of the scaffold from oxazole **6** to isoxazole **11** was not tolerated. Hence, the general skeleton and fatty acid mimetic structure³⁶ of **6** seemed favorable for Nurr1 modulator development and was retained for further SAR evaluation.

Table 1. Structural variation of the general scaffold.^a

ID	structure	Nurr1	RXR α	SI ^b
		IC ₅₀ [μ M] (rem. act.)	EC ₅₀ [μ M]	RXR α /Nurr1
6		40 \pm 6 (0.26 \pm 0.08) ^d	16.1 \pm 0.6 ^c	0.4
7		inactive (100 μ M)	inactive (30 μ M) ^c	-
8		inactive (100 μ M)	inactive (30 μ M) ^c	-
9		weak agonist ^e	inactive (30 μ M) ^e	-
10		56 \pm 12 (0.16 \pm 0.19)	inactive (50 μ M) ^e	>0.9
11		inactive (100 μ M)	inactive (100 μ M)	-

^a Cellular activities on Nurr1 and RXR α were determined in uniform Gal4 hybrid reporter gene assays. Data are the mean \pm S.E.M., n \geq 3. Remaining activity (rem. act.) refers to 0.1% DMSO treated cells. ^b The selectivity index (SI) was calculated by dividing the EC₅₀ for RXR α activation by the IC₅₀ for Nurr1 inhibition. ^c Activity data on RXR have been reported previously²⁶. ^d Activity data on Nurr1 have been reported previously²⁵. ^e Too toxic for characterization at higher concentrations.

Next, we studied the SAR around the two phenyl residues by systematically introducing additional substituents (Tables 2 and 3). Only few modifications were tolerated on the 4-phenyl moiety (**12–17**, Table 2) with 2-methyl (**12**), 3-chloro (**15**), 4-methyl (**16**) and 4-chloro (**17**) substituents fully disrupting activity. A methyl group in 3-position (**14**) was tolerated but the inactivity of the 3-chloro analogue **15** indicated no avenue to improvement in this position. Only a 2-chloro substituent (**13**) provided a slight improvement in potency but concomitantly diminished efficacy. This SAR was in strong contrast to RXR, where several structural variations on the 4-phenyl residue considerably promoted potency. The 4-phenyl motif hence seemed to hold little optimization potential towards selective Nurr1 modulation and we therefore turned our attention to the 5-phenyl residue.

Table 2. Evaluation of substituents on the 4-phenyl residue.^a

ID	R ¹	Nurr1	RXR α	SI ^b
		IC ₅₀ [μ M] (rem. act.)	EC ₅₀ [μ M]	RXR α /Nurr1
6	Ph	40 \pm 6 (0.26 \pm 0.08) ^d	16.1 \pm 0.6 ^c	0.4
12	2-CH ₃ -Ph	inactive (100 μ M)	6.5 \pm 0.1 ^c	-
13	2-Cl-Ph	14 \pm 8 (0.69 \pm 0.05)	36 \pm 1 ^c	2.6
14	3-CH ₃ -Ph	25 \pm 9 (0.25 \pm 0.12)	3.6 \pm 0.2 ^c	0.1
15	3-Cl-Ph	inactive (100 μ M)	1.9 \pm 0.2 ^c	-
16	4-CH ₃ -Ph	inactive (100 μ M)	9.9 \pm 0.9 ^c	-
17	4-Cl-Ph	inactive (100 μ M)	1.30 \pm 0.01 ^c	-

^a Cellular activities on Nurr1 and RXR α were determined in uniform Gal4 hybrid reporter gene assays. Data are the mean \pm S.E.M., $n\geq 3$. Remaining activity (rem. act.) refers to 0.1% DMSO treated cells. ^b The selectivity index (SI) was calculated by dividing the EC₅₀ for RXR α activation by the IC₅₀ for Nurr1 inhibition. ^c Activity data on RXR have been reported previously²⁶. ^d Activity data on Nurr1 have been reported previously²⁵.

The 5-phenyl substituent indeed tolerated more modifications (**18–28**, Table 3). Both a methyl group (**18**) and a chlorine atom (**19**) in 2-position caused a slight improvement in potency but also a loss in efficacy. Modification of the 3-position with a methyl (**20**) or a chloro substituent (**21**) was tolerated, too, with preference for the chlorine atom. In para-position, the same substituents disrupted inverse Nurr1 agonism (**22**, **23**). This SAR again markedly differed from RXR where modifications in 2-position had no effect while (lipophilic) derivatization in the 3- and 4-positions was highly favored²⁶. Substituents in 2-position hence emerged as an avenue to obtain selectivity for Nurr1 over RXR while the 3-position appeared to hold potential to improve potency. We explored this region further with alternative substituents but neither the 2- and 3-methoxy analogues (**24**, **25**), nor the 3-trifluoromethyl (**26**) derivative provided enhanced inverse Nurr1 agonism and also the 2,3-dichloro derivative **27** was less active than the mono-chloro analogues **19** and **21**. Based on the hypothesis that the higher potency of the ortho-substituted derivatives **18** and **19** might arise from a locked dihedral conformation, we evaluated the 2,6-dimethyl derivative **28** which would promote this effect, but **28** failed to suppress Nurr1 activity and rather acted as weak Nurr1 agonist.

Table 3. Evaluation of substituents on the 5-phenyl residue.^a

ID	R ²	Nurr1			RXR α		SI ^b RXR α /Nurr1
		IC ₅₀ [μ M] (rem. act.)		EC ₅₀ [μ M]			
6	Ph	40 \pm 6 (0.26 \pm 0.08) ^d		16.1 \pm 0.6 ^c		0.4	
18	2-CH ₃ -Ph	14 \pm 6 (0.75 \pm 0.06)		16.9 \pm 0.1 ^c		1.2	
19	2-Cl-Ph	15 \pm 7 (0.51 \pm 0.10)		17 \pm 1 ^c		1.1	
20	3-CH ₃ -Ph	> 50 μ M ^e		0.50 \pm 0.03 ^c		<0.1	
21	3-Cl-Ph	22 \pm 1 (0.54 \pm 0.04)		0.50 \pm 0.07 ^c		<0.1	
22	4-CH ₃ -Ph	inactive (100 μ M)		1.0 \pm 0.1 ^c		-	
23	4-Cl-Ph	inactive (100 μ M)		4.0 \pm 0.5 ^c		-	
24	2-CH ₃ O-Ph	> 50 μ M ^e		33 \pm 2		0.7	
25	3-CH ₃ O-Ph	> 50 μ M ^e		1.40 \pm 0.01 ^c		<0.1	
26	3-CF ₃ -Ph	> 50 μ M ^e		0.07 \pm 0.02 ^c		<0.1	
27	2,3-Cl ₂ -Ph	> 50 μ M ^e		1.20 \pm 0.01 ^c		<0.1	
28	2,6-(CH ₃) ₂ -Ph	weak agonist		4 \pm 1		-	

^a Cellular activities on Nurr1 and RXR α were determined in uniform Gal4 hybrid reporter gene assays. Data are the mean \pm S.E.M., $n\geq 3$. Remaining activity (rem. act.) refers to 0.1% DMSO treated cells. ^b The selectivity index (SI) was calculated by dividing the EC₅₀ for RXR α activation by the IC₅₀ for Nurr1 inhibition. ^c Activity data on RXR have been reported previously²⁶. ^d Activity data on Nurr1 have been reported previously²⁵. ^e Too toxic for characterization at higher concentrations.

Despite moderate improvements in potency and selectivity, modifications on the two phenyl substituents failed to open an avenue to major optimization of the oxaprozin scaffold as inverse Nurr1 agonist. Thus, we turned our attention to structural modifications in the propanoic acid side chain of **6** (Table 4) where variation of the carboxylic acid chain length enabled improvement in potency and selectivity towards Nurr1. While the shortest oxazolcarboxylic acid analogue **29** was equally potent as **6**, the oxazolylacetic acid **30** provided a substantial improvement in potency and the extended oxazolylbutyric acid **31** was likewise more active than **6**. The further elongated oxazolylpentanoic acid **32** comprised similar potency as **6** but weaker efficacy. This tolerance of various chain lengths by Nurr1 was attractive to achieve selectivity over RXR since chain shortening disrupted RXR agonism²⁶.

Encouraged by the beneficial impact of modifications in the acidic side chain on potency and selectivity, we probed further derivatization in this region of **6** (Table 4). A methyl group in α -position of the carboxylic acid moiety (**33**) slightly enhanced potency on Nurr1 suggesting further optimization potential. The corresponding α -ethyl (**34**) and α -isopropyl (**35**) analogues failed to exhibit enhanced inverse Nurr1 agonism but achieved improved selectivity over RXR. Rigidization of the propanoic acid chain of **6** in an acrylate motif (**36**) was highly preferred in terms of inverse Nurr1 agonism and enhanced potency and selectivity by a factor of ~ 10 . Introduction of the favored α -methyl group from **33** to the acrylate structure in **37**, a β -methyl group (**38**) and α,β -dimethyl substitution

(**39**) were not favored, however, and attempts to replace the acrylic acid by a bioisosteric *trans*- (**40**) or *cis*- (**41**) cyclopropanecarboxylic acid motif also resulted in reduced potency.

Table 4. Structural variation of the carboxylic acid side chain.^a

ID	R	Nurr1		RXR α		SI ^b RXR α /Nurr1
		IC ₅₀ [μ M] (rem. act.)		EC ₅₀ [μ M]		
6		40 \pm 6 (0.26 \pm 0.08) ^d		16.1 \pm 0.6 ^c		0.4
29		34 \pm 11 (0.36 \pm 0.12)		> 50 μ M ^c		>1.5
30		7 \pm 5 (0.37 \pm 0.21)		inactive (50 μ M)		>7.1
31		17 \pm 6 (0.40 \pm 0.10)		7.9 \pm 0.2 ^c		0.5
32		36 \pm 2 (0.64 \pm 0.02)		8.4 \pm 0.8 ^c		0.2
33		23 \pm 9 (0.21 \pm 0.14)		5.6 \pm 0.1		0.2
34		19 \pm 3 (0.51 \pm 0.04)		inactive (100 μ M)		>5.3
35		35 \pm 12 (0.13 \pm 0.15)		inactive (100 μ M)		>2.9
36		4.4 \pm 0.3 (0.01 \pm 0.03)		13 \pm 2		3.0
37		24 \pm 5 (0.0 \pm 0.2)		0.93 \pm 0.01		<0.1
38		50 \pm 15 (0.24 \pm 0.22)		10.4 \pm 0.4		0.2
39		70 \pm 7 (0.37 \pm 0.08)		1.2 \pm 0.1		<0.1
40		16 \pm 3 (0.41 \pm 0.06)		3.0 \pm 0.9		0.2
41		64 \pm 29 (0.19 \pm 0.23)		inactive (100 μ M)		>1.6

^a Cellular activities on Nurr1 and RXR α were determined in uniform Gal4 hybrid reporter gene assays. Data are the mean \pm S.E.M., n \geq 3. Remaining activity (rem. act.) refers to 0.1% DMSO treated cells. ^b The selectivity index (SI) was calculated by dividing the EC₅₀ for RXR α activation by the IC₅₀ for Nurr1 inhibition. ^c Activity data on RXR have been reported previously²⁶. ^d Activity data on Nurr1 have been reported previously²⁵.

Based on the rather flat SAR of the propanoic acid side chain and the PAINS character of the acrylic acid analogue **36** disqualifying this motif for further optimization, we next evaluated the SAR of the extended butyric acid analogue **31**. In addition to its favorable potency, this motif offered access to chain modifications with incorporation of heteroatoms to enhance polarity and simultaneously reduce binding affinity to the highly lipophilic RXR ligand binding site (Table 5). The latter was indeed evident from the oxazolymethylglycine derivative **42** which retained inverse Nurr1 agonism with similar potency as **6** but exhibited no activity on RXR. The tertiary *N*-methylglycine analogue **43** revealed no improvement over **42** pointing to little optimization potential of alternative *N*-substituents. Hence, we probed further amino acid conjugates (**44–47**), but introduction of the favored α -methyl substituent of **33** in the alanine conjugate **44** diminished inverse Nurr1 agonism and α -isobutyl (**45**), α -phenyl (**46**) and α -benzyl (**47**) moieties were also not favored. Chiral resolution and *in vitro* testing of **35** and **46** revealed no substantial differences between the respective enantiomers (Figure S1).

Table 5. Variation of the butanoic acid motif.^a

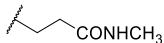
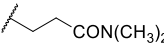
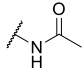
ID	R	Nurr1		RXR α		SI ^b	
		IC ₅₀ [μ M] (rem. act.)		EC ₅₀ [μ M]		RXR α /Nurr1	
31		17 \pm 6 (0.40 \pm 0.10)		7.9 \pm 0.2 ^c		0.5	
42		41 \pm 14 (0.4 \pm 0.1)		inactive (100 μ M)		>2.4	
43		46 \pm 12 (0.4 \pm 0.1)		inactive (100 μ M)		>2.2	
44		100 \pm 21 (0.37 \pm 0.16)		inactive (100 μ M)		>1.0	
45		69 \pm 10 (0.27 \pm 0.18)		inactive (100 μ M)		>1.4	
46		39 \pm 1 (0.29 \pm 0.01)		Inactive (100 μ M)		>2.6	
47		58 \pm 6 (0.41 \pm 0.09)		inactive (100 μ M)		>1.7	

^a Cellular activities on Nurr1 and RXR α were determined in uniform Gal4 hybrid reporter gene assays. Data are the mean \pm S.E.M., $n \geq 3$. Remaining activity (rem. act.) refers to 0.1% DMSO treated cells. ^b The selectivity index (SI) was calculated by dividing the EC₅₀ for RXR α activation by the IC₅₀ for Nurr1 inhibition. ^c Activity data on RXR have been reported previously²⁶.

After probing the SAR of the phenyl substituents as well as various propanoic and butyric side chain modifications, we studied the role of the carboxylic acid in **6** as remaining element for potential optimization (Table 6). Bioisosteric replacements of the carboxylic acid continued the trend of a flat SAR as the tetrazole **48**, oxadiazolone **49** and *N*-sulfonylamide **50** were equipotent to the carboxylic acid **6**. Despite not improving inverse Nurr1 agonism, these modifications consistently disrupted activity on RXR and thus improved selectivity. These observations further underline the divergent SAR of the oxaprozin scaffold as Nurr1 and RXR modulator demonstrating that inhibition of Nurr1 is not achieved indirectly via RXR activation. Amide replacement of the carboxylic acid was more productive in terms of improved inverse Nurr1 agonism. A primary amide (**51**) was tolerated with a loss in efficacy while the corresponding *N*-methyl amide (**52**) and the *N,N*-dimethyl amide **53** achieved remarkable efficacy blocking Nurr1 to only 4–6% remaining activity. Inversion of the amide (**54**) was also tolerated with strong inverse agonist efficacy.

Table 6. Variation of the carboxylic acid motif.^a

ID	R	Nurr1		RXR α		SI ^b	
		IC ₅₀ [μ M] (rem. act.)		EC ₅₀ [μ M]		RXR α /Nurr1	
6		40 \pm 6 (0.26 \pm 0.08) ^d		16.1 \pm 0.6 ^c		0.40	
48		43 \pm 4 (0.37 \pm 0.06)		inactive (100 μ M)		>2.3	
49		40 \pm 4 (0.37 \pm 0.04)		inactive (100 μ M)		>2.5	
50		28 \pm 10 (0.29 \pm 0.13)		inactive (100 μ M)		>3.6	
51		31 \pm 1 (0.75 \pm 0.01)		inactive (30 μ M) ^c		>1.0	

52		43±9 (0.04±0.14)	inactive (100 µM)	>2.3
53		26±3 (0.06±0.07)	inactive (100 µM)	>3.9
54		38±5 (0.12±0.10)	inactive (100 µM)	>2.6

^a Cellular activities on Nurr1 and RXR α were determined in uniform Gal4 hybrid reporter gene assays. Data are the mean±S.E.M., n≥3. Remaining activity (rem. act.) refers to 0.1% DMSO treated cells. ^b The selectivity index (SI) was calculated by dividing the EC₅₀ for RXR α activation by the IC₅₀ for Nurr1 inhibition. ^c Activity data on RXR have been reported previously²⁶. ^d Activity data on Nurr1 have been reported previously²⁵.

After systematic SAR elucidation for all parts of the oxaprozin scaffold as inverse Nurr1 agonist (summarized in Figure 1), we eventually aimed to combine the obtained knowledge in fused derivatives focusing on modifications that provided improved potency (Table 7). **55** comprising the 2-chlorophenyl motif in 5-position (**19**) and the *N,N*-dimethylpropanamide (**53**) revealed no additive improvement in potency. Similarly, incorporation of the favored α -methyl group of **33** in the propanamide (**56**) and fusion of the acrylate (**36**) and *N,N*-dimethylamide (**53**) motifs failed to enhance inverse Nurr1 agonism (**57**). For the shorter oxazolylacetic acid scaffold of **30**, fusion with the 5-(2-chlorophenyl) residue of **19** or the *N,N*-dimethylamide of **53** was also not productive (**58–60**).

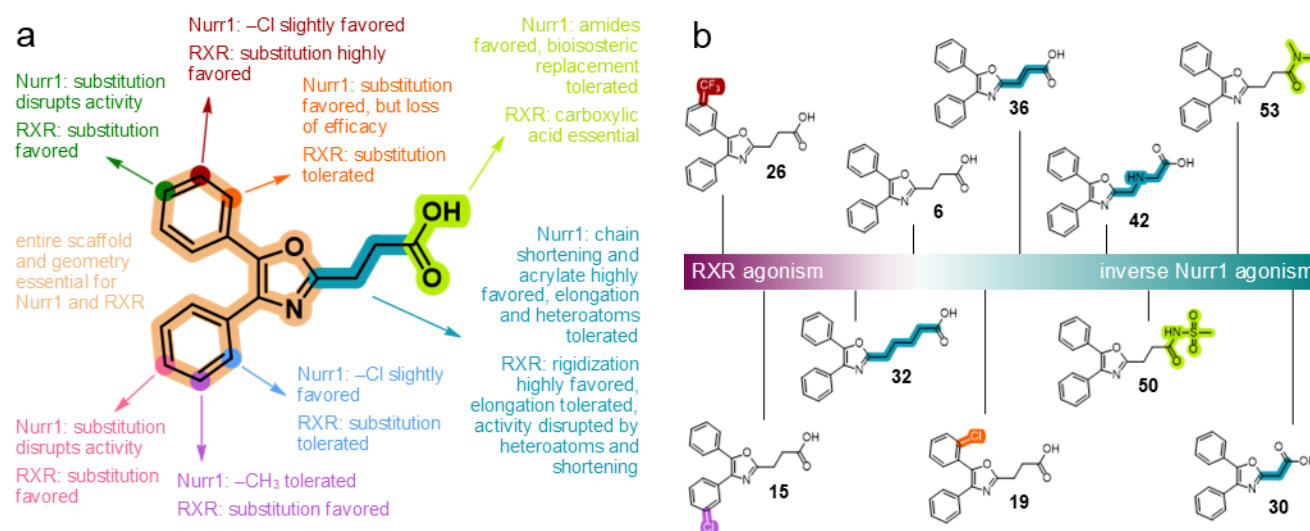


Figure 1. Summary of the divergent SAR of oxaprozin-based Nurr1 and RXR ligands (a) and exemplary oxaprozin derivatives with selective or dual activity on RXR and Nurr1 (b).

These results further underscore the restrictive SAR of the oxaprozin scaffold as Nurr1 modulator and the challenge in the development of inverse Nurr1 agonists. Nevertheless, extensive and systematic SAR evaluation of **6** yielded several selective inverse Nurr1 agonists with improved potency and remarkable efficacy in blocking Nurr1 activity. Based on these characteristics, compounds **30**, **36**, **53** and **55** emerge as leads for further optimization and as potential early tools to study the biology of Nurr1. This was also supported by ligand efficiency metrics (Table 8) characterizing **30**, **36**, **53** and **55** as improved inverse Nurr1 agonists compared to the lead **6**. These compounds were hence broadly characterized for Nurr1 binding and modulation as well as for their selectivity profiles in the nuclear receptor family.

Table 7. Fusion of favored modifications.^a

ID	structure	Nurr1	RXR α	SI ^b
		IC ₅₀ [μ M] (rem. act.)	EC ₅₀ [μ M]	RXR α /Nurr1
55		24 \pm 2 (0.26 \pm 0.06)	inactive (50 μ M) ^c	>2.1
56		33 \pm 2 (0.16 \pm 0.09)	inactive (100 μ M)	>3.0
57		12 \pm 1 (0.27 \pm 0.03)	inactive (100 μ M)	>8.3
58		13 \pm 3 (0.46 \pm 0.05)	inactive (100 μ M)	>7.7
59		52 \pm 8 (0.20 \pm 0.09)	inactive (100 μ M)	>1.9
60		17 \pm 4 (0.60 \pm 0.05)	inactive (100 μ M)	>5.9

^a Cellular activities on Nurr1 and RXR α were determined in uniform Gal4 hybrid reporter gene assays. Data are the mean \pm S.E.M., n \geq 3. Remaining activity (rem. act.) refers to 0.1% DMSO treated cells. ^b The selectivity index (SI) was calculated by dividing the EC₅₀ for RXR α activation by the IC₅₀ for Nurr1 inhibition. ^c Too toxic for characterization at higher concentrations.

Table 8. Efficiency metrics of inverse Nurr1 agonists.^a

ID	IC ₅₀ (Nurr1)	LE	LLE ^b	SILE
6	40 \pm 6 μ M	0.27	0.37	1.74
30	7 \pm 5 μ M	0.34	1.52	2.07
36	4.4 \pm 0.3 μ M	0.33	1.25	2.12
53	26 \pm 3 μ M	0.26	0.56	1.77
55	24 \pm 2 μ M	0.25	-0.06	1.76

^a Metrics ligand efficiency (LE), lipophilic ligand efficiency (LLE), and size-independent ligand efficiency (SILE) were calculated as described in ref. ³⁷. ^b SlogP for LLE was calculated with RDkit.

For orthogonal validation of direct Nurr1 modulation, we studied the interaction of **30**, **36**, **53** and **55** with the Nurr1 LBD by isothermal titration calorimetry (ITC) which demonstrated robust binding with K_D values between 0.3 μ M and 1.0 μ M (Table 9, Figure 2a). To capture effects on Nurr1 in a more physiological setting than the hybrid reporter gene assay, we also evaluated modulation of full-

length human Nurr1 on its three response elements NBRE, NurRE and DR5 by **30**, **36**, **53** and **55** (Table 9). All four inverse Nurr1 agonists consistently blocked the activity of Nurr1 as monomer (NBRE), homodimer (NurRE) and RXR-heterodimer (DR5). In line with the results from the hybrid reporter gene assay, the acrylic acid **36** was the most potent inverse Nurr1 agonist while **53** exhibited the strongest efficacy in Nurr1 inhibition.

Table 9. Nurr1 binding affinity and biological activity of 30, 36, 53, and 55 on human full-length Nurr1.^a

Nurr1 IC ₅₀ [μM] (rem. act.)				
ID	NBRE (monomer)	NurRE (homodimer)	DR5 (heterodimer)	K _D (Nurr1 LBD)
6	12±2 (0.20±0.05) ^b	17±3 (0.27±0.05) ^b	12±2 (0.27±0.05) ^b	n.d.
30	10±2 (0.57±0.03)	12±2 (0.37±0.04)	10±4 (0.55±0.07)	0.3 μM
36	3±1 (0.75±0.05)	5.3±0.3 (0.42±0.03)	4±1 (0.74±0.06)	0.6 μM
53	12±3 (0.49±0.07)	25±4 (0.18±0.09)	18±6 (0.52±0.08)	1.0 μM
55	13±5 (0.51±0.11)	26±7 (0.29±0.04)	12±3 (0.64±0.08)	0.6 μM

^a Data are the mean±S.E.M., n≥3. ^b Activity data for **6** have been reported previously²⁵.

Table 10. Activity profile of 30, 36, 53, and 55 on the NR4A family receptors.^a

IC ₅₀ [μM] (rem. act.)			
ID	Nurr1	Nur77	NOR-1
6	40±6 (0.26±0.08) ^b	16±5 (0.2±0.1) ^b	22±4 (≥ 0.00) ^b
30	7±5 (0.37±0.21)	8±4 (0.59±0.06)	10±2 (0.46±0.03)
36	4.4±0.3 (0.01±0.03)	1.9±0.5 (0.22±0.09)	3.8±0.2 (0.09±0.03)
53	26±3 (0.06±0.07)	37±5 (0.10±0.11)	39±5 (0.22±0.08)
55	24±2 (0.26±0.06)	20±1 (0.20±0.03)	29±4 (0.25±0.04)

^a Inverse agonist activity on Nurr1, Nur77, and NOR-1 was determined in uniform cellular Gal4 hybrid reporter gene assays. Data are the mean±S.E.M., n≥3. ^b Activity data for **6** have been reported previously²⁵.

Generating selectivity over RXR was a key objective of this study and achieved with the inverse Nurr1 agonists **30**, **36**, **53** and **55**. However, the typical fatty acid mimetic structure of oxaprozin and derivatives suggests potential interaction also with other related receptors^{36,38} and we hence profiled the activity of the optimized compounds on fatty acid and lipid-sensing nuclear receptors (Figure 2b). **30**, **36**, **53** and **55** were favorably selective and only revealed slight agonism on peroxisome proliferator-activated receptors (PPARs) as off-target activity which was most pronounced for the shortened oxaprozin analogue **30**. On the NR4A receptors Nur77 and NOR-1, **30**, **36**, **53** and **55** expectedly exhibited similar activity as on Nurr1 (Table 10). Previous evaluation of the scaffold as cyclooxygenase (COX) inhibitor demonstrated that increasing the length and/or branching of the alkanolic side chain and replacement of the carboxylic acid by an amide and was not tolerated³⁹. The amide derivatives **53**, **55** and **58** were thus favored in terms of Nurr1 preference over COX inhibition. This was also supported by computational target prediction using a consensus of three publicly available tools⁴⁰⁻⁴² which generally suggested favorable selectivity profiles (Figure S2).

To evaluate the suitability of the oxaprozin-derived inverse Nurr1 agonist scaffold for *in vivo* studies, we evaluated pharmacokinetic parameters of selected compounds *in vitro* (Figure 2c-e, Table 11). Predicted PK properties (SwissADME^{43,44}) were generally favorable with high bioavailability and brain penetration scores (Table 11). This was also evident in a parallel artificial membrane permeability assay (PAMPA) revealing similarly high membrane permeation of the amides **53**, **55**, **57**, and **58** as the reference drug propranolol (Figure 2c, Table 11). The lead **6** and **36** were slightly less permeable. A cellular blood-brain-barrier (BBB) model additionally indicated comparable brain penetration of the amide **53** and the brain-penetrant reference antipyrine⁴⁵ offering an improvement over the lead **6** (Figure 2d). Moreover, *in vitro* microsomal stability tests demonstrated long half-lives for **6** and the corresponding unsaturated derivative **36** (Figure 2e). The amides **53**, **55**, **57**, and **58** revealed lower resistance against microsomal degradation but sufficient stability of **53**, **57**, and **58** to be used as tools. Only **55** was rapidly degraded.

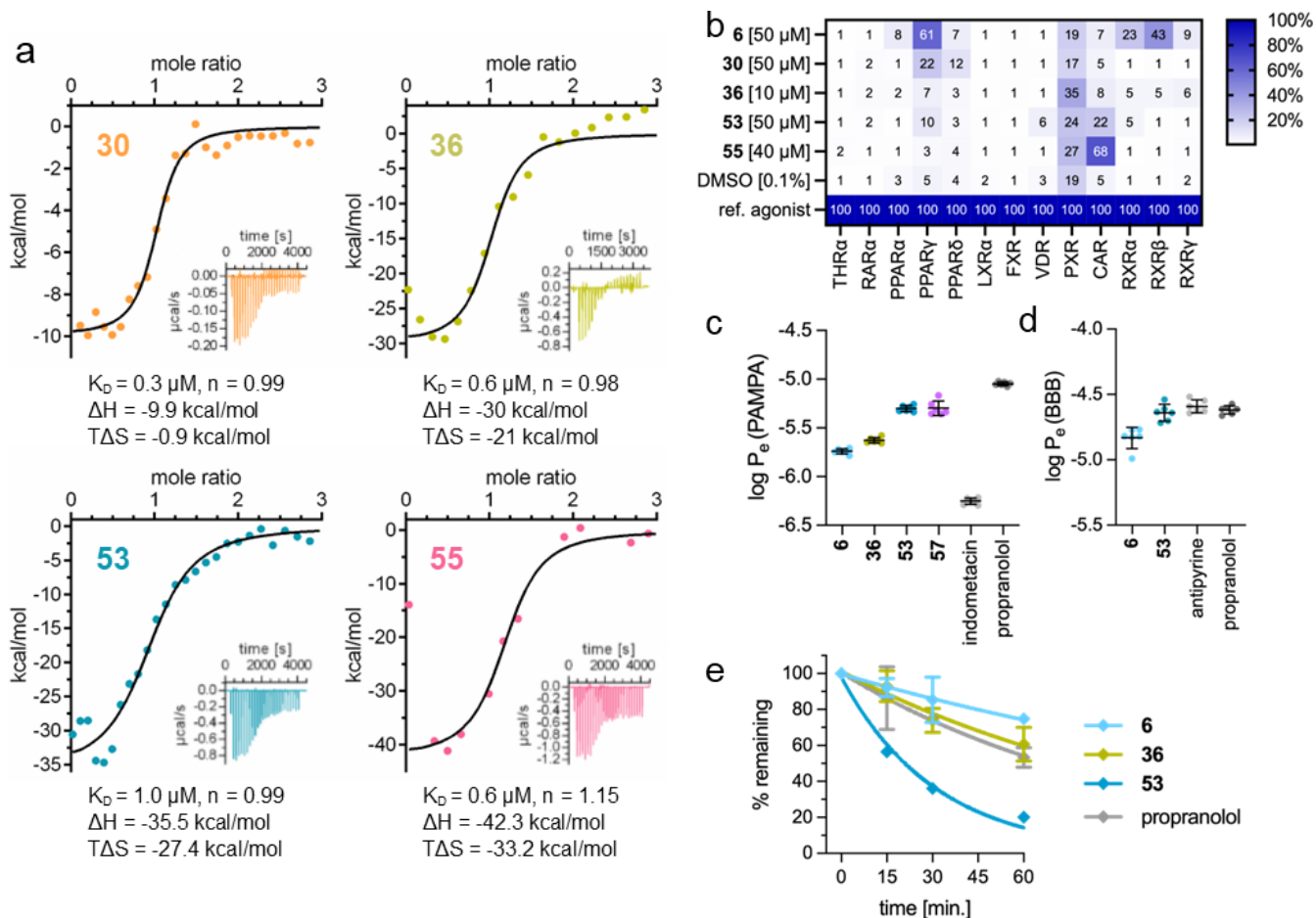


Figure 2. Profiling of **30**, **36**, **53**, **55**, and **57**. (a) Isothermal titration calorimetry (ITC) demonstrated binding of **30**, **36**, **53** and **55** to the Nurr1 LBD with (sub-)micromolar affinities. The major panels show the fitting of the blank-corrected heat of binding and the minor panels show the isotherms of the compound–protein titrations. (b) Selectivity screening among fatty acid and lipid-sensing nuclear receptors determined in HEK293T cells using Gal4-hybrid reporter gene assays. Respective reference agonists (1 μM each) are listed in experimental section. Heatmap shows the mean relative activation vs. ref. agonist, $n \geq 3$. (c) Permeability of inverse Nurr1 agonists in a parallel artificial membrane permeability assay (PAMPA). Indometacin and propranolol for comparison. Data are the mean \pm SD; $n=6$. (d) Ability of **6** and **53** to cross a cellular model of the blood-brain-barrier (BBB). Antipyrine and propranolol for comparison. Data are the mean \pm SD; $n=6$. (e) Stability of **6**, **36**, and **53** against degradation by rat liver microsomes. Propranolol for comparison. Data are mean \pm SD remaining compound [%] after the indicated incubation time; $n=3$.

Table 11. *In vitro* PK properties.

ID	predicted ^a				experimental		
	BBB permeant	GI absorption	P-gp substrate	bioavailability score	logPe (PAMPA) ^c	logPe (BBB model) ^d	microsomal half-live [min] ^b
6	yes	high	no	0.85	-5.74 \pm 0.03	-4.83 \pm 0.08	141 \pm 8
36	yes	high	no	0.85	-5.63 \pm 0.03	n.d.	88 \pm 13
53	yes	high	no	0.55	-5.30 \pm 0.03	-4.64 \pm 0.06	21.6 \pm 0.4
55	yes	high	no	0.55	-5.10 \pm 0.08	n.d.	8.9 \pm 0.4
57	yes	high	no	0.55	-5.30 \pm 0.07	n.d.	30 \pm 3
58	yes	high	no	0.55	-5.27 \pm 0.02	n.d.	26 \pm 1
propranolol	yes	high	no	0.55	-5.05 \pm 0.02	-4.62 \pm 0.03	64 \pm 4

^a Predictions from SwissADME^{43,44}. ^b Stability against degradation by rat liver microsomes was determined by LCMS. Data are the mean \pm SD, $n=3$. ^c Permeability was determined in a parallel artificial membrane permeability assay. Data are the mean \pm SD, $n=6$. ^d Penetration of the blood-brain-barrier (BBB) was determined in a cellular BBB model. Data are the mean \pm SD, $n=6$. n.d. - not determined.

Nurr1 modulation with ligands is poorly understood from a structural perspective⁴⁶ and only few ligand bound co-crystal structures are available. To establish a binding site hypothesis for the inverse Nurr1 agonists derived from **6**, we employed the close relative Nur77 of Nurr1, which has been co-crystallized with several modulators binding to four different sites within its LBD and mapped these regions to Nurr1 for docking. While no reasonable binding modes of **6** were predicted for three surface pockets derived from Nur77 (not shown), we observed potential interaction with the PGA1 binding site (Figure 3a). This observation agreed with the original hypothesis of mimicking the COX metabolite PGA1 in the binding site¹³ with COX inhibitors which led to the discovery of NSAIDs like **6** as NR4A modulators²⁵. Docking of **6** to the Nurr1:PGA1 complex (PDB ID 5Y41) suggested binding between helices 4/5, 11 and 12 with polar contacts of the carboxylic acid motif to Arg515 and the backbone of His516 similar to PGA1. The 4,5-diphenyloxazole protruded towards the hydrophobic pocket accommodating the lipophilic tail of PGA1.

The predicted binding to the PGA1 site also aligned well with our SAR observations: Increased potency of the acrylic acid analog **36** could be rationalized by its higher rigidity and preorientation of the carboxylic acid to engage contacts with Arg515 and His516 (Figure 3b). Moreover, the relative solvent exposure of the aliphatic chain of the scaffold supported the lack of an eutomer for the chiral analogs **35** and **46** which formed similar poses for both absolute configurations (Figure 3c, d and Figure S3a) with the bulky substituents oriented towards the solvent.

In an attempt to validate the computationally predicted binding *in vitro*, we performed mutagenesis of Leu444 which is located in the putative inverse agonist binding pocket but not involved in contacts to the activation function thus suggesting that its mutation would not alter Nurr1 activity but could affect ligand binding. As one phenyl motif of the inverse agonist scaffold was predicted to bind close to Leu444, we hypothesized an additional edge-to-face π -interaction between ligand and mutant Nurr1-L444F which was supported by modelling (Figure 3e, Figure S3c). *In vitro* validation indeed revealed 3- to 4-fold higher potency of **6** and selected derivatives (**32**, **53**) on Nurr1-L444F (Figure 3f) providing further support for the predicted binding epitope.

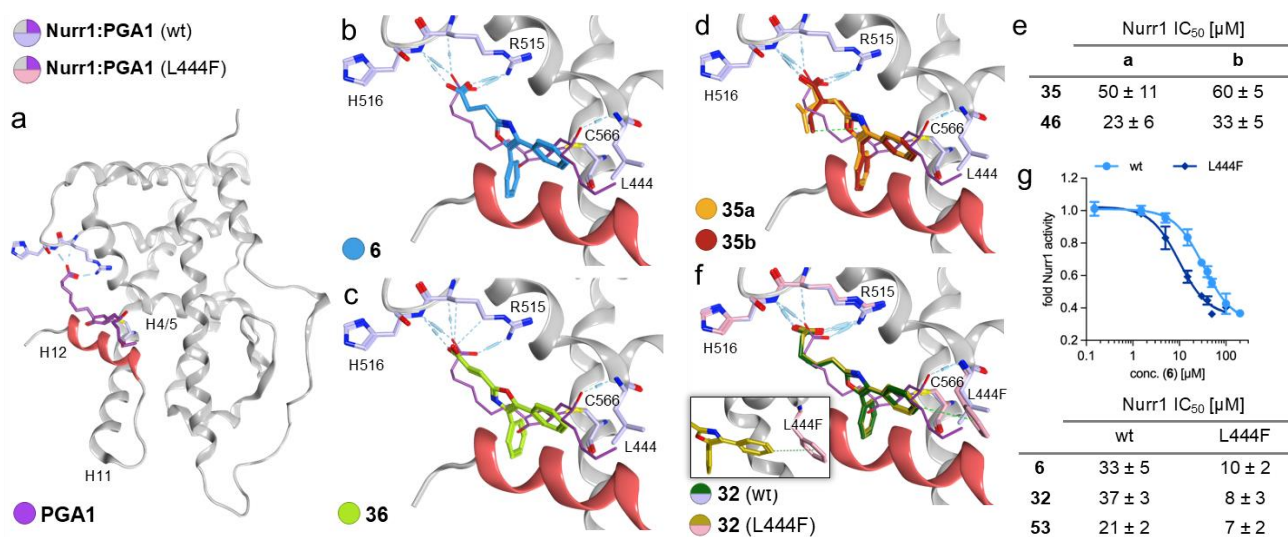


Figure 3. *In silico* and *in vitro* studies on the potential binding site of inverse Nurr1 agonists within the Nurr1 LBD. (a) Overview of location of the PGA1 binding site within the Nurr1 LBD. Activation function 2 located in helix 12 is highlighted in red. (b) Docking of **6** to the Nurr1:PGA1 complex (PDB ID 5Y41) suggested binding with polar contacts of the carboxylic acid motif similar to PGA1. (c) Enhanced potency of **36** was likely due to higher rigidity of the side chain compared to the flexible alkyl linker and optimal preorientation of the carboxylic acid for contacts with Arg515 and His516. (d) Docking of both absolute configurations of the chiral derivative **35** to the Nurr1:PGA1 complex suggested no relevant difference in binding of the enantiomers. Docking of enantiomers of **46** in Figure S3a. (e) Activity of the enantiomers of **35** and **46** in the Nurr1-Gal4 reporter gene assay suggesting no eutomer. Data are the mean±S.E.M.; n≥3. (f) Docking of **32** to the Nurr1:PGA1 complex (purple) and the L444F mutant (rose) suggested an additional edge-to-face contact with the mutant Phe. (g) Inverse agonist potency of **6**, **32**, and **53** on the Nurr1-L444F mutant was increased by a factor of ~3–4 compared to wild-type, supporting interaction with the proposed binding epitope. Data are the mean±S.E.M.; n≥3.

While Nurr1 agonism has recently advanced with potent agonists^{16,21,47} and *in vitro* pharmacological studies^{16,47}, the biological impact of inverse Nurr1 agonism remained elusive. Despite moderate potency, the inverse agonists **36**, **53** and **55** emerged with robust Nurr1 inhibition (1–26% remaining activity) as early chemical tools to further explore Nurr1 pharmacology. As Nurr1 is considered as key neuroprotective transcription factor, we studied inverse agonist effects in rat dopaminergic neurons (N27)⁴⁸. Inverse agonist treatment at concentrations around IC₅₀ values did not induce pronounced apoptosis or necrosis but inhibited N27 cell proliferation in a dose-dependent manner (Figure 4, Figure S4) and strongly sensitized the cells to the neurotoxin 6-hydroxydopamine (6-OHDA). A sublethal 6-OHDA dose (6 μM) did not counteract proliferation but unfolded pronounced antiproliferative effects in presence of inverse

agonists. This synergistic effect of neurotoxin treatment and concomitant Nurr1 inhibition aligns with Nurr1's neuroprotective role. Closer inspection of these effects revealed that neuronal apoptosis was consistently enhanced by combined inverse agonist and neurotoxin treatment (Figure 4b, e and Figure S4b, d). Importantly, these effects of inverse Nurr1 agonists were not observed in an enterocyte cell line (HT29) which in contrast to N27 cells express very low Nurr1 levels (Figure 4c, Figure S5).⁴⁹ In contrast to the consistent effects of inverse Nurr1 agonists, the reference agonist **4** did not alter N27 proliferation in presence or absence of 6-OHDA (Figure 4f, g). These preliminary phenotypic results point to anti-proliferative effects of pharmacological Nurr1 inhibition in neural cells which is in line with the proposed role of Nurr1 in the maintenance of maturing and adult midbrain dopamine neurons⁵⁰ and in the survival of ventral mesencephalic late dopaminergic precursor neurons⁵¹.

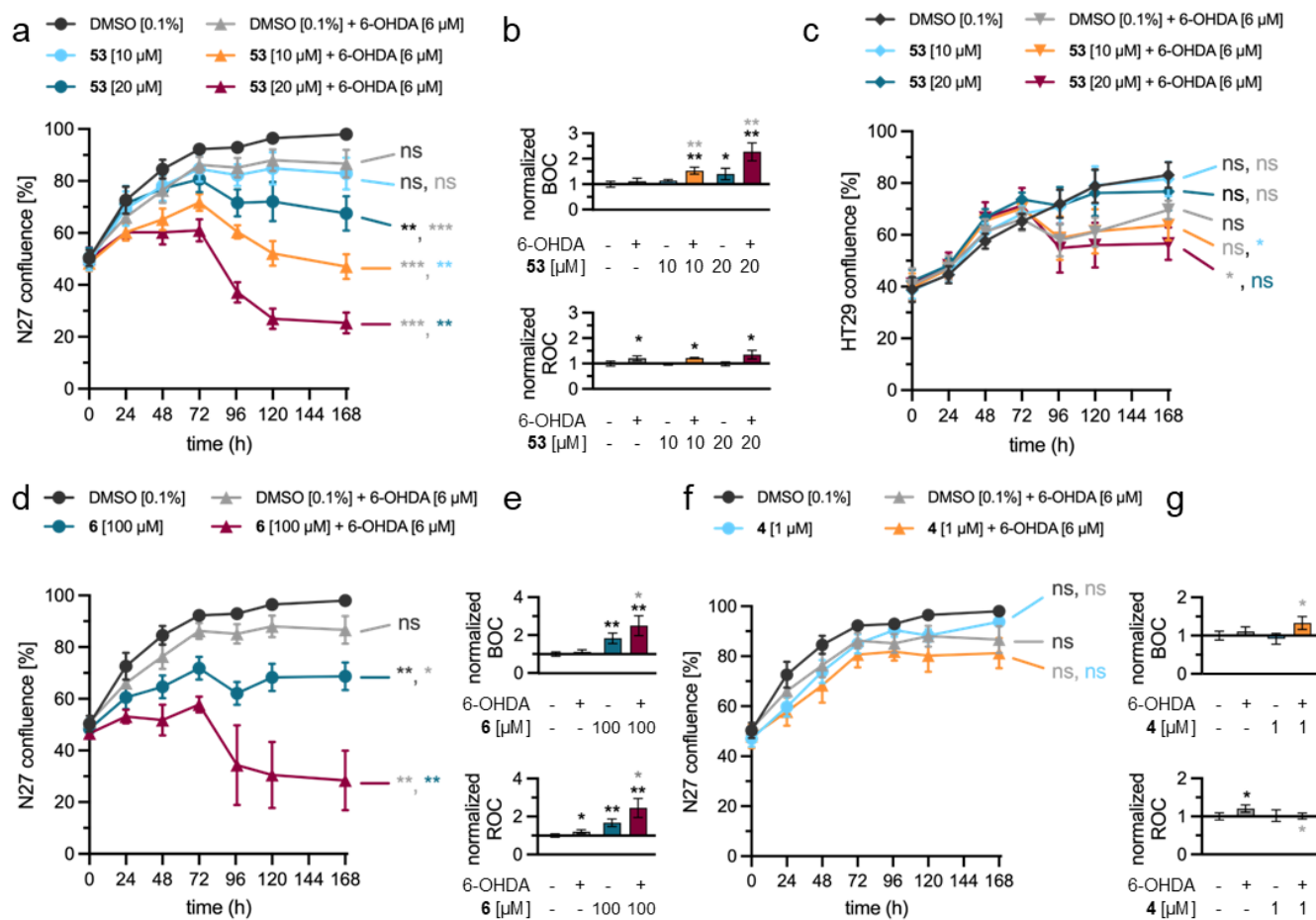


Figure 4. Inverse agonist treatment (**6**, **53**) sensitized rat dopaminergic neuronal cells (N27) to the neurotoxin 6-hydroxydopamine (6-OHDA) and altered proliferation. (a, d) Proliferation curves of N27 rat dopaminergic neurons treated with inverse agonists **53** (a) or **6** (d) with or without a sub-toxic concentration of 6-OHDA (6 μ M). (b, e) Impact of N27 treatment with **53** (b) or **6** (e) with or without 6 μ M 6-OHDA for 24 h apoptosis (blue object count, BOC) and necrosis (red object count, ROC). (c) Proliferation curves of HT29 enterocytes treated with **53** with or without 6 μ M 6-OHDA. (f, g) Effects of Nurr1 agonist **4** on proliferation (f) and apoptosis and necrosis (g) of N27 cells for comparison. Data are the mean \pm SD; n=4. * p<0.05, ** p<0.01, *** p<0.001 (two-way ANOVA (proliferation at 168 h) or unpaired two-sided t-test). Asterisks are colored respective to the data point their significance is referring to. BOC and ROC are normalized on confluence.

Conclusion

As an approved drug, oxaprozine (**6**) offers drug-like properties per definition and is an attractive lead structure for the development of Nurr1 modulators following the selective optimization of side-activities (SOSA)^{52,53} concept. As a critical step in this endeavor, we aimed to obtain oxaprozine-derived Nurr1 modulators exhibiting selectivity over RXR. We have performed an extensive systematic SAR study on **6** as Nurr1 and RXR modulator addressing all structural elements of the chemotype. The SAR of **6** on Nurr1 and RXR diverged substantially, and although Nurr1 was rather restrictive, we succeeded in identifying various structural modifications driving selectivity for Nurr1 over RXR. These findings enabled the design of inverse Nurr1 agonists with no activity on RXR and demonstrate that inhibition of Nurr1 activity is not a secondary effect of RXR modulation.

In line with the SOSA concept, we focused on small structural modifications which failed to provide a major improvement in inverse Nurr1 agonist potency. Further optimization may require a scaffold hop or incorporation of greater structural changes and will also have to address the lack of selectivity over the related receptors Nur77 and NOR1. Nevertheless, the inverse Nurr1 agonists obtained from oxaprozine are endowed with sub-micromolar binding affinity, robust inhibition of Nurr1 activity at low micromolar concentrations and favorable PK properties and thus provide a substantial advance over previously available compounds. *In silico* and *in vitro* binding studies on oxaprozine-derived inverse Nurr1 agonists enabled a robust binding site hypothesis in a pocket located behind the activation helix 12 which contributes to molecular understanding of Nurr1 and may aid future computer-aided Nurr1 ligand design. Moreover, application of oxaprozine-derived inverse Nurr1 agonists in phenotypic experiments in N27 rat dopaminergic neurons revealed anti-proliferative and neurotoxin-sensitizing effects of pharmacological Nurr1 inhibition further supporting the transcription factor's neuroprotective role.

Experimental Section

Chemistry

General. All chemicals were of reagent grade, purchased from commercial sources (e.g., Sigma-Aldrich, abcr, Enamine and BLDpharm) and used without further purification unless otherwise specified. Test compound **6** was obtained from TCI, test compound **7** was acquired from Sigma Aldrich, test compound **9** was obtained from Prestwick Chemical Libraries, and test compounds **10** and **52–54** were acquired from Enamine Ltd. All reactions were conducted in oven-dried glassware under Ar atmosphere and in absolute solvents. Other solvents, especially for work-up procedures, were of reagent grade or purified by distillation (isohexane, EtOAc, EtOH). Reactions were monitored by thin layer chromatography (TLC) on TLC Silica gel 60 F254 aluminum sheets by Merck and visualized under ultraviolet light (254 nm) or by in-process LC/MS. Purification by column chromatography (CC) was either performed using silica gel (40–60 μ m) or performed on a puriFlash® XS520Plus system (Advion Inc., Ithaca, NY, USA) using high performance spherical silica columns (SIHP, 50 μ m) by Interchim. Reverse phase CC was performed on a puriFlash® 5.250 system (Advion) using C18HP columns (SIHP, 15 μ m) by Interchim and a gradient of 0.1% formic acid in H₂O to 100% acetonitrile (HPLC gradient grade). Or semi-preparative purification was performed on a LCMS 2020 (Shimadzu, Duisburg, Germany) using a Luna 10 μ C18(2) (250 \times 21.20 nm)-column from Phenomenex LTD Deutschland (Aschaffenburg, Germany). As eluent mixtures of acetonitrile/0.1% aqueous formic acid were used, with a flow rate of 21 mL/min at r.t.. The following methods were used: linear gradient from 50 to 90% ACN over 10 min, 90% ACN for 5 min, linear gradient from 90 to 50% ACN over 1 min, 50% for 2 min (method A); 5% ACN over 2 min, linear gradient from 5% to 90% ACN over 12 min, 90% ACN for 6 min, linear gradient from 90% to 5% ACN over 1 min, 50% for 4 min (method B). NMR spectra were recorded on Bruker AV 300, Bruker AV 400, Bruker AV 500, Bruker Avance III HD 400, or Bruker Avance III HD 500 spectrometers (Bruker Corporation, Billerica, MA, USA). Deuterated solvents DMSO-*d*₆, CDCl₃, Acetone-*d*₆, and MeOD-*d*₄ used for NMR spectroscopy were purchased and used without further drying. Chemical shifts (δ) are reported in ppm relative to TMS as reference or residual solvent signal protons. Approximate coupling constants (*J*) are shown in Hertz (Hz). Mass spectra were obtained on a VG Platform II (Thermo Fischer Scientific, Inc., Waltham, MA, USA) using electrospray ionization (ESI) or on an Advion expression™ CMS (Advion) using atmospheric pressure chemical ionization (APCI) or on a LCMS 2020 (Shimadzu) equipped with an ESI-TOF. High resolution mass spectra were recorded on a MALDI LTQ ORBITRAP XL instrument or on a LTQ FT instrument for electrospray ionization (ESI) (Thermo Fisher Scientific) or on a Finnigan MAT 95 spectrometer (Thermo Fisher Scientific) using electron impact ionization (EI) at a source temperature of 250 °C and an electron energy of 70 eV with a method dependent range from 40 to 1040 u. Compound purity was analyzed either by HPLC-UV, HPLC-MS or qHNMR quantification. For HPLC-UV, purity was analyzed either on a Waters 600 Controller HPLC using a Waters 2487 Dual Absorbance Detector and Waters 717 plus Autosampler or on a Hitachi Chromaster with a 5160 pump system, using a DAD 5430 and 5260 Autosampler both equipped with a MultoHigh100 RP18-5 μ 250 \times 4 mm column (CS-Chromatographie Service GmbH, Langerwehe, Germany) using a gradient (H₂O+0.1% formic acid/MeOH 80:20 isocratic for 5 min to MeOH after additional 45 min and MeOH for additional 10 min) at a flow rate of 1 mL/min and UV-detection at 254 nm and 280 nm (method C) or using a gradient (H₂O+0.1% formic acid/MeOH 60:40 isocratic for 5 min to MeOH after additional 25 min and MeOH for additional 10 min) at a flow rate of 1 mL/min and UV-detection at 245 nm and 280 nm (method D). Or, HPLC-UV purity was analyzed on a LCMS 2020 (Shimadzu) using a Luna 10u C18(2) (250 \times 4.6 nm)-column from (Phenomenex LTD Deutschland). The system is equipped with a SPD 20A UV/VIS detector (λ = 240/280 nm) and an ESI-TOF (measuring in the positive- and/or negative-ion mode). As eluent mixtures of acetonitrile/0.1% aqueous formic acid were used, with a flow rate of 0.1 mL/min at r.t.. The following method was used: linear gradient from 50 to 90% ACN over 10 min, 90% ACN for 5 min, linear gradient from 90 to 50% ACN over 1 min, 50% for 2 min (method A). Purity of the compounds was determined by integrating the peaks of the UV-chromatogram. Quantitative ¹H NMR (qHNMR) were acquired according to a method described by Pauli *et al.*⁵⁴ with internal calibration. The qHNMR measurements were carried out under conditions allowing complete relaxation to assure the exact determination of peak area ratios. All final compounds for biological evaluation had a purity of >95% according to qHNMR or to HPLC-MS or to HPLC-UV analysis at wavelengths 254 and 280 nm. Synthesis and analytical characterization of **11**, **24**, **28**, **33–35**, **42–50**, **55–60**, and their precursors are described in the Supporting Information.

***In vitro* Assays**

Hybrid Reporter Gene Assays. *Plasmids:* The Gal4-fusion receptor plasmids pFA-CMV-hNurr1-LBD²⁵, pFA-CMV-hRXR α -LBD⁵⁵, pFA-CMV-hRXR β -LBD⁵⁵, pFA-CMV-hRXR γ -LBD⁵⁵, pFA-CMV-hNur77-LBD²⁵, pFA-CMV-hNOR1-LBD²⁵, pFA-CMV-hTHR α -LBD⁵⁶, pFA-CMV-hRAR α -LBD⁵⁵, pFA-CMV-hPPAR α -LBD⁵⁷, pFA-CMV-hPPAR γ -LBD⁵⁷, pFA-CMV-hPPAR δ -LBD⁵⁷, pFA-CMV-hLXR α -LBD⁵⁸, pFA-CMV-hFXR-LBD⁵⁹, pFA-CMV-hVDR-LBD⁵⁵, pFA-CMV-hPXR-LBD⁵⁵, and pFA-CMV-hCAR-LBD⁵⁵ coding for the hinge region and ligand binding domain of the canonical isoform of the respective human nuclear receptor have been reported previously. The Gal4-VP16⁶⁰ fusion protein expressed from plasmid pECE-SV40-Gal4-VP16⁶¹ (Addgene plasmid #71728, Watertown, MA, USA) served as ligand-independent transcriptional inducer for control experiments. pFR-Luc (Stratagene, La Jolla, CA, USA) was used as reporter plasmid and pRL-SV40 (Promega, Madison, WI, USA) for normalization of transfection efficiency and test compound toxicity. *Assay procedure:* HEK293T cells (German Collection of Microorganisms and Cell Culture GmbH, DSMZ) were cultured in Dulbecco's modified Eagle's medium (DMEM), high glucose supplemented with 10% fetal calf serum (FCS), sodium pyruvate (1 mM), penicillin (100 U/mL), and streptomycin (100 μ g/mL) at 37 °C and 5% CO₂ and seeded in 96-well plates (3 \times 10⁴ cells/well). After 24 h, the medium was changed to Opti-MEM without supplements, and cells were transiently transfected using Lipofectamine LTX reagent (Invitrogen, Carlsbad, CA, USA) according to the manufacturer's protocol. Five hours after transfection, cells were incubated with the test compounds in Opti-MEM supplemented with penicillin (100 U/mL), streptomycin (100 μ g/mL), and 0.1% dimethyl sulfoxide (DMSO) for 16 h before luciferase activity was measured using the Dual-Glo Luciferase Assay System (Promega) according to the manufacturer's protocol on a Tecan Spark luminometer (Tecan Group AG, Männedorf, Switzerland). Firefly luminescence was divided by Renilla luminescence and multiplied by 1000 resulting in relative light units (RLU) to normalize for transfection efficiency and cell growth. Fold activation was obtained by dividing the test compound by the mean RLU of the untreated control. Max. relative activation refers to fold reporter activation of a test compound divided by the fold activation of the respective reference agonist (THR α : T3; RAR α : tretinoin; PPAR α : GW7647; PPAR γ : pioglitazone; PPAR δ : L165041; LXR α : T0901317; FXR: GW4064; VDR: calcitriol; PXR: Rifampicin; CAR: CITCO; RXR $\alpha/\beta/\gamma$: bexarotene; all at a concentration of 1 μ M; Nurr1: amodiaquine (2, 100 μ M)). All hybrid assays were validated with the above-mentioned reference agonists which yielded EC₅₀ values in agreement with the literature. All samples were tested in at least three biologically independent experiments in duplicate. The Gal4-VP16 control experiment was carried out in duplicates as well, with at least four independent repeats. For dose-response curve fitting and calculation of IC₅₀/EC₅₀ values, the equation "[Inhibitor]/[Agonist] vs response - variable slope (four parameters)" was used in GraphPad Prism (version 7.00, GraphPad Software, La Jolla, CA, USA). Activity of test compounds on the Nurr1-L444F mutant was determined as described for wild-type Gal4-Nurr1 using pFA-CMV-hNurr1-L444F-LBD, which was constructed by site-directed mutagenesis using the Phusion Site-Directed Mutagenesis Kit (Thermo Scientific) and the following mutagenesis primer sequences: Pho-5'-TCG TAC CCT TAG CAC ACA GGG-3' and Pho-5'-AGT TCT GGG AGC TTC CCC AAC AGT TT-3'.

Full-Length Nurr1 Reporter Gene Assays. *Plasmids:* The reporter plasmids pFR-Luc-NBRE²⁵, pFR-Luc-NurRE²⁵, and pFRLuc-DR5²⁵ each containing one copy of the respective human Nurr1 response element NBRE NI3 (TGATATCGAAAACA~~AAAGGTCA~~), NurRE (from POMC; TGATATTTACCTCCAAATGCCA), or DR5 (TGATAGGTTCCACCGAAAGGTCA) were described previously. The full length human nuclear receptor Nurr1 (pcDNA3.1-hNurr1-NE; Addgene, entry 102363) and, for DR5, RXR α (pSG5-hRXR⁶²) were overexpressed. pFL-SV40 (Promega) was used for normalization of transfection efficiency and evaluation of compound toxicity. *Assay procedure:* HEK293T cells were grown in DMEM high glucose, supplemented with 10% FCS, sodium pyruvate (1 mM), penicillin (100 U/mL), and streptomycin (100 μ g/mL) at 37°C and 5% CO₂. The day before transfection, HEK293T cells were seeded in 96-well plates (3 \times 10⁴ cells/well). The medium was changed to Opti-MEM without supplements right before transfection. Transient transfection was performed using the Lipofectamine LTX reagent (Invitrogen) according to the manufacturer's protocol with pFR-Luc-NBRE²⁵, pFR-Luc-NurRE²⁵ or pFR-Luc-DR5²⁵, pRL-SV40 (Promega), the human full length receptor plasmid pcDNA3.1-hNurr1-NE, and, for DR5, also pSG5-hRXR⁶². Five hours after transfection, the medium was changed to Opti-MEM supplemented with penicillin (100 U/mL) and streptomycin (100 μ g/mL), now additionally containing 0.1% DMSO and the respective test compound or 0.1% DMSO alone as untreated control. Each sample was tested in duplicates and each experiment was performed independently three times. Following 16 h incubation with the test compounds, the cells were assayed for luciferase activity using the Dual-GloTM Luciferase Assay System (Promega) according to the manufacturer's protocol. Luminescence was measured with a Spark 10 M luminometer (Tecan Group AG). Normalization of transfection efficiency and cell growth were done by division of firefly luciferase data by renilla luciferase data and multiplying the value by 1000 resulting in RLU. Fold activation was obtained by dividing the mean RLU of a test compound at a respective concentration by the mean RLU of untreated control. The full length Nurr1 reporter gene assays were validated with amodiaquine (2) and chloroquine as reference agonists.

Recombinant Expression and Purification of Nurr1 LBD Protein. The Nurr1 LBD (aa 362–598) was subcloned into pNIC28-Bsa4. The recombinant protein containing an N-terminal His₆-tag was expressed in Escherichia coli BL21(DE3)-R3-pRARE2, cultured in TB. Expression was induced with 0.5 mM IPTG at 18 °C overnight. The protein was purified by Ni²⁺-affinity chromatography followed by TEV treatment to remove the histidine tag. The cleaved protein was further purified by reverse Ni²⁺-affinity chromatography and size exclusion chromatography.

Isothermal Titration Calorimetry. ITC experiments were conducted on an Affinity ITC instrument (TA Instruments, New Castle, DE, USA) at 25 °C with a stirring rate of 75 rpm. Nurr1 LBD protein (15–20 μ M) in buffer (20 mM Tris, pH 7.5, 100 mM NaCl, 5% glycerol) containing 5% DMSO was titrated with the test compounds (60–100 μ M in the same buffer containing 1–4% DMSO) in 21–26 injections (1 \times 1 μ L and 20–25 \times 4 μ L) with an injection interval of 150 s. As control experiments, the test compounds were titrated to the buffer, and the buffer was titrated to the Nurr1 LBD protein under otherwise identical conditions. The heats of the

compound–protein titrations were corrected with the heats of the compound–buffer titrations and analyzed using NanoAnalyze software (version 3.11.0, TA Instruments) with independent binding models.

Parallel Artificial Membrane Permeability Assay (PAMPA). Passive lipid membrane diffusion of test compounds was determined using Merck Millipore MultiScreen Filter Plates (0.45 μm pore diameter, hydrophobic PVDF). The filter inserts were coated with 1% L- α -phosphatidylcholine (Fluka Analytical) in *n*-dodecan. The test compounds were then added to the donor compartment at a final concentration of 500 μM in a phosphate buffer pH 7.4 containing 5% DMSO with a total volume of 150 μL . The acceptor compartment was filled with 300 μL PBS containing 5% DMSO. Additionally, three equilibrium samples were prepared by directly adding the donor solution to the acceptor compartment for the calculation of log Pe values. The filter plates were incubated for 18 h before the test compound concentrations in the acceptor compartments and in the equilibrium samples were determined by UV absorbance at 285 nm (**6** and **53**), 245 nm (**57**), 250 nm (**55**), 260 nm (indomethacin), 280 nm (**58**), 290 nm (propranolol), and 310 nm (**36**) with external calibration in a 96 well quartz plate on a SpectraMax M2e microplate reader (Molecular Devices, LLC, San Jose, CA, USA). logPe values were calculated according to the formula published by Sugano et al⁶³.

In vitro Blood-Brain-Barrier Model. Permeation of test compounds through a human brain endothelial cell barrier was evaluated using the Corning Costar 3470 Transwell Plate system (0.4 μm pore diameter with 6.5 mm inserts) and HBEC-5i cells (ATCC, CRL-3245). Filter inserts were coated one day before seeding with 50 μL 0.01% rat-tail collagen type I (C7661, Sigma-Aldrich) in PBS. 60,000 HBEC-5i cells in 100 μL HBEC-5i-medium (DMEM/F12 with 10% FCS and 40 $\mu\text{g}/\text{mL}$ ECGS) were seeded after aspiration of the coating-supernatant in each insert with 600 μL HBEC-5i-medium in each receiver well. After 24 h incubation at 37 $^{\circ}\text{C}$ with 5% CO_2 , medium was exchanged to 600 μL T98G cell supernatant in receiver wells and 100 μL fresh HBEC-5i-medium in inserts. The medium exchange was repeated every second day. On day 7 after seeding, medium in the receiver wells was replaced by 600 μL Hank's balanced salt solution (HBSS) containing 10 mM HEPES and 0.1% DMSO and 100 μL test compound mixtures (antipyrine, propranolol and test compound; each at 10 μM) in HBSS containing 10 mM HEPES and 0.1% DMSO were added to inserts. After 60 min incubation, 100 μL samples were taken from the receiver wells and diluted in 400 μL (75%/25% A/B; A=Formic acid 0.1% in water; B=MeCN). Test compound concentrations in the samples were determined by LC-MS/MS on an API-3200-QTrap (Sciex) equipped with an Agilent Technologies 1100 series setup including a binary pump (G1311A), a degasser (G1322A), and a Shimadzu SIL 20A HT autosampler under the control of Analyst 1.6 (Sciex). An XBridge BEH C18 (3.5 μm , 150 mm x 3 mm, Waters, protected with a 0.5 μm frit) served as stationary phase in combination with a gradient method starting with 0.1% formic acid in water (A) and MeCN (B) as mobile phase (80%:20% = A:B) for 6 min going to (50%:50%) after 8 min. 5 μL of aspirated supernatant diluted in mobile phase starting conditions was loaded onto the column, separated at a flow rate of 400 $\mu\text{L}/\text{min}$, and quantified per Area of MRM (multiple reaction monitoring).

Microsomal Stability Assay. To assess the microsomal stability, the test compounds (10 μM) were incubated in 100 mM potassium phosphate-based buffer at pH 7.4 (total volume of 100 μL) containing 0.5 mg/mL male rat liver microsomes (Sprague-Dawley, #M9066, Sigma Aldrich) and 1 mM NADPH for 0, 15, 30, or 60 min. At the end of the incubation time, microsomal activity was terminated by addition of 500 μL MeCN, subsequent centrifugation at 1700g for 5 minutes. A reaction mixture containing heat-inactivated microsomes (95 $^{\circ}\text{C}$, 10 min) served as a matrix control. 5 μL supernatant of each sample were analyzed and the remaining concentrations of the respective test compounds at each time point was determined by LC-MS/MS on an API-3200-QTrap (Sciex) with an Agilent Technologies 1100 series setup including a binary pump (G1311A), a degasser (G1322A), and a Shimadzu SIL 20A HT autosampler under the control of Analyst 1.6 (Sciex). A XBridge BEH C18 (3.5 μm , 150 mm x 3 mm, Waters, protected with a 0.5 μm frit) stationary phase was used in combination with a gradient method starting with 0.1% formic acid in water (A) and MeCN (B) as mobile phase (A:B = 80:20) for 6 min going to A:B = 50:50 after 8 min. 5 μL of supernatant diluted in mobile phase starting conditions was loaded onto the column, separated at a flow rate of 400 $\mu\text{L}/\text{min}$, and detected and quantified per Area of MRM (multiple reaction monitoring) with the following transitions: 293.932/103.100 Da (**6**); 291.919/165.100 Da (**36**); 320.909/103.100 Da (**53**); 354.812/309.800 Da (**55**); 318.887/273.900 Da (**57**); 306.902/102.900 Da (**58**). Data are expressed as means \pm SD of single determinations obtained in three independent experiments. For determination of half-lives the remaining compound [%] values after the indicated incubation time [min] were used in the equation “one phase decay” in GraphPad Prism (version 10, GraphPad Software).

Proliferation Assay. N27 rat dopaminergic neural cells (SCC048, Sigma-Aldrich, Darmstadt, Germany) were cultured in RPMI 1640 medium (Gibco, Thermo Fisher Scientific, Waltham, MA, USA) supplemented with 10% FCS, penicillin (100 U/mL), and streptomycin (100 $\mu\text{g}/\text{mL}$) at 37 $^{\circ}\text{C}$ and 5% CO_2 . The cells were seeded in transparent 96-well plates (5×10^3 cells/well). After 24 h, the medium was changed to RPMI 1640 medium supplemented with 0.1% FCS, penicillin (100 U/mL), and streptomycin (100 $\mu\text{g}/\text{mL}$) additionally containing 0.1% DMSO and test compounds **4** (1 μM), **6** (100 μM), **36** (10, 30 μM), **53** (10, 20 μM) or **55** (10, 30 μM) or 0.1% DMSO alone, as well as either 6-hydroxydopamine (6 μM , Sigma-Aldrich) or no neurotoxin as unstressed control (200 $\mu\text{L}/\text{well}$). The test compound containing medium was refreshed after 96 h (200 $\mu\text{L}/\text{well}$). Each concentration was tested in duplicates and the experiment was performed independently four times. Cell confluence was assessed on a Tecan Spark Cyto (Tecan Group AG) for 7 days starting from first incubation with test compounds ($t = 0$ h). As a non-neuronal control cell line, HT29 colon adenocarcinoma cells (a kind gift from Prof. Angelika Vollmar (Ludwig-Maximilians University, Munich, Germany)) were used. HT29 cells were cultured in McCoy's modified 5A medium (Gibco) supplemented with 10% FCS, penicillin (100 U/mL), and streptomycin (100 $\mu\text{g}/\text{mL}$) at 37 $^{\circ}\text{C}$ and 5% CO_2 . The cells were seeded in transparent 96-well plates (7.5×10^3 cells/well). After 24 h, the medium was changed to McCoy's modified 5A medium supplemented with 0.1% FCS, penicillin (100 U/mL), and streptomycin (100 $\mu\text{g}/\text{mL}$) additionally containing 0.1% DMSO and test compound **53** (10, 20 μM) or 0.1% DMSO alone, as well as either with 6-hydroxydopamine (6 μM , Sigma-Aldrich) or without neurotoxin as unstressed control (200 $\mu\text{L}/\text{well}$). The proliferation assay over 7 days was otherwise performed as described above for N27 cells.

Cytotoxicity Assay. N27 rat dopaminergic neural cells (SCC048) were grown in RPMI 1640 medium (Gibco) supplemented with 10% FCS, penicillin (100 U/mL), and streptomycin (100 µg/mL) at 37 °C and 5% CO₂ and seeded in 96-well plates (1 × 10⁴ cells per well). After 24 h, medium was changed to RPMI 1640 medium, supplemented with 0.1% FCS, penicillin (100 U/mL), and streptomycin (100 µg/mL) additionally containing 0.1% DMSO and test compounds **4** (1 µM), **6** (100 µM), **36** (10, 30 µM), **53** (10, 20 µM) or **55** (10, 30 µM) or 0.1% DMSO alone, as well as either 6-hydroxydopamine (6 µM, Sigma-Aldrich) or no neurotoxin as unstressed control. Each sample was tested in duplicates and the experiment was performed independently four times. Induction of apoptotic and necrotic cell death was assessed after 24 h of incubation by staining with NucView® 405 Blue Caspase-3 Dye (Sigma-Aldrich) and Live-or-Dye Nuc-Fix™ Red (0.05x, Biotium, Inc., Fremont, CA, USA), respectively. After light-protected incubation for 30 min, confluence as well as apoptotic and necrotic cell count were determined via brightfield and fluorescence imaging (blue fluorescence channel: Ex: 381–400 nm, Em: 414–450 nm; red fluorescence channel: Ex: 543–566 nm, Em: 580–611 nm) on a Tecan Spark Cyto (Tecan Group AG).

Computational Procedures

General. Calculations were performed in MOE (version 2022.02, Chemical Computing Group ULC, Montreal, QC, Canada) using default settings for each tool and function unless stated otherwise. Amber10:EHT was used as the default force field for all calculations.

Molecular Docking. Docking was performed using the X-ray structure of the Nurr1 LBD in complex with PGA1 (PDB ID: 5Y41). Protonation state of the complex was adjusted using the MOE QuickPrep tool. The compounds were prepared using the Energy minimize tool with preserved existing chirality and MOE Wash tool: protonation state dominant at pH 7.0. Docking was performed using the following settings in the MOE Dock tool: receptor: receptor+solvent; site: ligand atoms; placement: Triangle Matcher; score: London dG; poses: 100; refinement: Induced Fit; refinement score: GBVI/WSA dG; poses: 10. The ten top-ranking poses were analyzed. For docking to the L444F mutant of the complex, the respective residue in the Nurr1:PGA1 complex (PDB ID: 5Y41) was changed manually using the MOE Builder panel and minimizing the potential energy of the obtained structure prior to docking with the same settings as described above.

Associated content

Supporting Information (pdf) contains synthetic procedures, and analytical data of **11, 24, 28, 33–35, 42–50, 55–60**.

Author information

Corresponding Authors

* sabine.willems@cup.lmu.de

* daniel.merk@cup.lmu.de

Notes

The authors declare no competing financial interests.

Acknowledgment

This research was co-funded by the European Union (ERC, NeuRoPROBE, 101040355). Views and opinions expressed are however those of the author(s) only and do not necessarily reflect those of the European Union or the European Research Council. Neither the European Union nor the granting authority can be held responsible for them. This research was supported by the European Union in the Erasmus+ Traineeship Mobility of M.B. (project no. 2020-1-IT02-KA103-078486). Gal4-VP16 was a gift from Lea Sistonen (Addgene plasmid #71728). pcDNA3.1-hNurr1-NE was a gift from Shu Leong Ho (Addgene plasmid #102363).

Abbreviations

AD, Alzheimer's Disease; ANOVA, analysis of variance; AQ, amodiaquine; BBB, blood-brain-barrier; BOC, blue object count; CAR, constitutive androstane receptor; CC, column chromatography; CNS, central nervous system; DHI, 5,6-dihydroxyindole; DR5, Nurr1-RXR heterodimer response element; EAE, experimental autoimmune encephalomyelitis; FXR, farnesoid X receptor; GI, gastrointestinal; ITC, isothermal titration calorimetry; LBD, ligand binding domain; LE, ligand efficiency; LLE, lipophilic ligand efficiency; LXR, liver X receptor; MPTP, 1-methyl-4-phenyl-1,2,3,6-tetrahydropyridine; MS, multiple sclerosis; NBRE, Nurr1 monomer response element; NSAID, non-steroidal anti-inflammatory drug; Nurr1, Nuclear receptor related 1; NurRE, Nurr1 homodimer response element; PAINS, pan-assay interference compounds; PAMPA, parallel artificial membrane permeability assay; PD, Parkinson's Disease; P-gp, P-glycoprotein; PPAR, peroxisome proliferator-activated receptor; PXR, pregnane X receptor; RAR, retinoic acid receptor; ROC, red object count; RXR, retinoid X receptor; SAR, structure-activity relationship; SI, selectivity index; SILE, size-independent ligand efficiency; SOSA, selective optimization of side-activities; THR, thyroid hormone receptor; VDR, vitamin D receptor; VP16, Herpes simplex virus protein vmw65.

References

- Wang, Z.; Benoit, G.; Liu, J.; Prasad, S.; Aarnisalo, P.; Liu, X.; Xu, H.; Walker, N. P. C.; Perlmann, T. Structure and Function of Nurr1 Identifies a Class of Ligand-Independent Nuclear Receptors. *Nature* **2003**, *423* (6939), 555–560.
- Willems, S.; Zaienne, D.; Merk, D. Targeting Nuclear Receptors in Neurodegeneration and Neuroinflammation. *J. Med. Chem.* **2021**, *64* (14), 9592–9638.
- Alexander, S. P.; Cidlowski, J. A.; Kelly, E.; Marrion, N. V.; Peters, J. A.; Faccenda, E.; Harding, S. D.; Pawson, A. J.; Sharman, J. L.; Southan, C.; Davies, J. A. THE CONCISE GUIDE TO PHARMACOLOGY 2017/18: Nuclear Hormone Receptors. *Br. J. Pharmacol.* **2017**, *174*, S208–S224.
- Decressac, M.; Volakakis, N.; Björklund, A.; Perlmann, T. NURR1 in Parkinson Disease - From Pathogenesis to Therapeutic Potential. *Nat. Rev. Neurol.* **2013**, *9* (11), 629–636.
- Liu, W.; Gao, Y.; Chang, N. Nurr1 Overexpression Exerts Neuroprotective and Anti-Inflammatory Roles via down-Regulating CCL2 Expression in Both in Vivo and in Vitro Parkinson's Disease Models. *Biochem. Biophys. Res. Commun.* **2017**, *482* (4), 1312–1319.
- Moon, M.; Jeong, I.; Kim, C.-H.; Kim, J.; Lee, P. K. J.; Mook-Jung, I.; Leblanc, P.; Kim, K.-S. Correlation between Orphan Nuclear Receptor Nurr1 Expression and Amyloid Deposition in 5XFAD Mice, an Animal Model of Alzheimer's Disease. *J. Neurochem.* **2015**, *132* (2), 254–262.
- Moon, M.; Jung, E. S.; Jeon, S. G.; Cha, M.-Y.; Jang, Y.; Kim, W.; Lopes, C.; Mook-Jung, I.; Kim, K.-S. Nurr1 (NR4A2) Regulates Alzheimer's Disease-Related Pathogenesis and Cognitive Function in the 5XFAD Mouse Model. *Aging Cell* **2019**, *18* (1), e12866.
- Satoh, J.; Nakanishi, M.; Koike, F.; Miyake, S.; Yamamoto, T.; Kawai, M.; Kikuchi, S.; Nomura, K.; Yokoyama, K.; Ota, K.; Kanda, T.; Fukazawa, T.; Yamamura, T. Microarray Analysis Identifies an Aberrant Expression of Apoptosis and DNA Damage-Regulatory Genes in Multiple Sclerosis. *Neurobiol. Dis.* **2005**, *18* (3), 537–550.
- Montarolo, F.; Perga, S.; Martire, S.; Bertolotto, A. Nurr1 Reduction Influences the Onset of Chronic EAE in Mice. *Inflamm. Res.* **2015**, *64* (11), 841–844.
- Jakaria, M.; Haque, M. E.; Cho, D.-Y.; Azam, S.; Kim, I.-S.; Choi, D.-K. Molecular Insights into NR4A2(Nurr1): An Emerging Target for Neuroprotective Therapy Against Neuroinflammation and Neuronal Cell Death. *Mol. Neurobiol.* **2019**, *56* (8), 5799–5814.
- Bruning, J. M.; Wang, Y.; Oltrabella, F.; Tian, B.; Kholodar, S. A.; Liu, H.; Bhattacharya, P.; Guo, S.; Holton, J. M.; Fletterick, R. J.; Jacobson, M. P.; England, P. M. Covalent Modification and Regulation of the Nuclear Receptor Nurr1 by a Dopamine Metabolite. *Cell Chem. Biol.* **2019**, *26* (5), 674–685.e6.
- de Vera, I. M. S.; Giri, P. K.; Munoz-Tello, P.; Brust, R.; Fuhrmann, J.; Matta-Camacho, E.; Shang, J.; Campbell, S.; Wilson, H. D.; Granados, J.; Gardner, W. J.; Creamer, T. P.; Solt, L. A.; Kojetin, D. J. Identification of a Binding Site for Unsaturated Fatty Acids in the Orphan Nuclear Receptor Nurr1. *ACS Chem. Biol.* **2016**, *11* (7), 1795–1799.
- Rajan, S.; Jang, Y.; Kim, C.-H.; Kim, W.; Toh, H. T.; Jeon, J.; Song, B.; Serra, A.; Lescar, J.; Yoo, J. Y.; Beldar, S.; Ye, H.; Kang, C.; Liu, X.-W.; Feitosa, M.; Kim, Y.; Hwang, D.; Goh, G.; Lim, K.-L. et al. PGE1 and PGA1 Bind to Nurr1 and Activate Its Transcriptional Function. *Nat. Chem. Biol.* **2020**, *16* (8), 876–886.
- Kim, C.-H.; Han, B.-S.; Moon, J.; Kim, D.-J.; Shin, J.; Rajan, S.; Nguyen, Q. T.; Sohn, M.; Kim, W.-G.; Han, M.; Jeong, I.; Kim, K.-S.; Lee, E.-H.; Tu, Y.; Naffin-Olivos, J. L.; Park, C.-H.; Ringe, D.; Yoon, H. S.; Petsko, G. A. et al. Nuclear Receptor Nurr1 Agonists Enhance Its Dual Functions and Improve Behavioral Deficits in an Animal Model of Parkinson's Disease. *Proc. Natl. Acad. Sci.* **2015**, *112* (28), 8756–8761.
- Munoz-Tello, P.; Lin, H.; Khan, P.; de Vera, I. M. S.; Kamenecka, T. M.; Kojetin, D. J. Assessment of NR4A Ligands That Directly Bind and Modulate the Orphan Nuclear Receptor Nurr1. *J. Med. Chem.* **2020**, *63* (24), 15639–15654.
- Kim, W.; Tripathi, M.; Kim, C.; Vardhini, S.; Cha, Y.; Kandi, S. K.; Feitosa, M.; Kholiya, R.; Sah, E.; Thakur, A.; Kim, Y.; Ko, S.; Bhatia, K.; Manohar, S.; Kong, Y.-B.; Sindhu, G.; Kim, Y.-S.; Cohen, B.; Rawat, D. S. et al. An Optimized Nurr1 Agonist Provides Disease-Modifying Effects in Parkinson's Disease Models. *Nat. Commun.* **2023**, *14*, 4283.
- Willems, S.; Ohrndorf, J.; Kilu, W.; Heering, J.; Merk, D. Fragment-like Chloroquinolineamines Activate the Orphan Nuclear Receptor Nurr1 and Elucidate Activation Mechanisms. *J. Med. Chem.* **2021**, *64* (5), 2659–2668.
- Kholodar, S. A.; Lang, G.; Cortopassi, W. A.; Iizuka, Y.; Brah, H. S.; Jacobson, M. P.; England, P. M. Analogs of the Dopamine Metabolite 5,6-Dihydroxyindole Bind Directly to and Activate the Nuclear Receptor Nurr1. *ACS Chem. Biol.* **2021**, *16* (7), 1159–1163.
- Vietor, J.; Gege, C.; Stiller, T.; Busch, R.; Schallmayer, E.; Kohlhof, H.; Höfner, G.; Pabel, J.; Marschner, J. A.; Merk, D. Development of a Potent Nurr1 Agonist Tool for In Vivo Applications. *J. Med. Chem.* **2023**, *66* (9), 6391–6402.
- Ballarotto, M.; Willems, S.; Stiller, T.; Nawa, F.; Marschner, J. A.; Grisoni, F.; Merk, D. De Novo Design of Nurr1 Agonists via Fragment-Augmented Generative Deep Learning in Low-Data Regime. *J. Med. Chem.* **2023**, *66* (12), 8170–8177.
- Sai, M.; Vietor, J.; Kormmayer, M.; Egner, M.; López-García, Ú.; Höfner, G.; Pabel, J.; Marschner, J. A.; Wein, T.; Merk, D. Structure-Guided Design of Nurr1 Agonists Derived from the Natural Ligand Dihydroxyindole. *J. Med. Chem.* **2023**, *66* (19), 13556–13567.
- Xue, X.; Soroosh, P.; De Leon-Tabaldo, A.; Luna-Roman, R.; Sablad, M.; Rozenkrants, N.; Yu, J.; Castro, G.; Banie, H.; Fung-Leung, W. P.; Santamaria-Babi, L.; Schlueter, T.; Albers, M.; Leonard, K.; Budelsky, A. L.; Fourie, A. M. Pharmacologic Modulation of ROR γ t Translates to Efficacy in Preclinical and Translational Models of Psoriasis and Inflammatory Arthritis. *Sci. Rep.* **2016**, *6*, 37977.
- Gege, C. Retinoic Acid-Related Orphan Receptor Gamma t (ROR γ t) Inverse Agonists/Antagonists for the Treatment of Inflammatory Diseases - Where Are We Presently? *Expert Opin. Drug Discov.* **2021**, *16* (12), 1517–1535.
- Zaienne, D.; Willems, S.; Schierle, S.; Heering, J.; Merk, D. Development and Profiling of Inverse Agonist Tools for the Neuroprotective Transcription Factor Nurr1. *J. Med. Chem.* **2021**, *64* (20), 15126–15140.
- Willems, S.; Kilu, W.; Ni, X.; Chaikuad, A.; Knapp, S.; Heering, J.; Merk, D. The Orphan Nuclear Receptor Nurr1 Is Responsive to Non-Steroidal Anti-Inflammatory Drugs. *Commun. Chem.* **2020**, *3*, 85.
- Schierle, S.; Chaikuad, A.; Lillich, F. F.; Ni, X.; Woltersdorf, S.; Schallmayer, E.; Renelt, B.; Ronchetti, R.; Knapp, S.; Proschak, E.; Merk, D. Oxaprozin Analogues as Selective RXR Agonists with Superior Properties and Pharmacokinetics. *J. Med. Chem.* **2021**, *64* (8), 5123–5136.
- Kramer, J. S.; Woltersdorf, S.; Dufflot, T.; Hiesinger, K.; Lillich, F. F.; Knöll, F.; Wittmann, S. K.; Klingler, F.-M.; Brunst, S.; Chaikuad, A.; Morisseau, C.; Hammock, B. D.; Buccellati, C.; Sala, A.; Rovati, G. E.; Leuillier, M.; Fraigneau, S.; Rondeaux, J.; Hernandez-Olmos, V. et al. Discovery of the First in Vivo Active Inhibitors of the Soluble Epoxide Hydrolase Phosphatase Domain. *J. Med. Chem.* **2019**, *62* (18), 8443–8460.
- Talley, J. J. Isoxazole Compounds as Cyclooxygenase Inhibitors. US5859257A. *G. D. Searle Co.* **1999**.
- Imai, S.; Kikui, H.; Moriyama, K.; Togo, H. One-Pot Preparation of 2,5-Disubstituted and 2,4,5-Trisubstituted Oxazoles from Aromatic Ketones with Molecular Iodine, Oxone, and Trifluoromethanesulfonic Acid in Nitriles. *Tetrahedron* **2015**, *71* (33), 5267–5274.
- Patil, P. C.; Luzzio, F. A. Synthesis of Extended Oxazoles II: Reaction Manifold of 2-(Halomethyl)-4,5-Diaryloxazoles. *Tetrahedron Lett.* **2016**, *57* (7), 757–759.
- White, K. N.; Konopelski, J. P. Facile Synthesis of Highly Functionalized N-Methyl Amino Acid Esters without Side-Chain Protection. *Org. Lett.* **2005**, *7* (19), 4111–4112.
- Ram, S.; Spicer, L. D. Debenzylation of N-Benzylamino Derivatives by Catalytic Transfer Hydroxylation With Ammonium Formate. *Synth. Commun.* **1987**, *17* (4), 415–418.
- Wu, G.; Yin, W.; Shen, H. C.; Huang, Y. One-Pot Synthesis of Useful Heterocycles in Medicinal Chemistry Using a Cascade Strategy. *Green Chem.* **2012**, *14* (3), 580–585.
- Mangette, J. E.; Johnson, M. R.; Le, V.-D.; Shenoy, R. A.; Roark, H.; Stier, M.; Belliotti, T.; Capiris, T.; Guzzo, P. R. The Preparation of Optically

- Active α -Amino 4H-[1,2,4]Oxadiazol-5-Ones from Optically Active α -Amino Acids. *Tetrahedron* **2009**, *65* (46), 9536–9541.
- (35) Bregman, H.; Chakka, N.; Dimauro, E. F.; Gao, H.; Gunaydin, H.; Huang, H.; Olivieri, P.; Schenkel, L.; Weiss, M. Biaryl Acyl-Sulfonamide Compounds as Sodium Channel Inhibitors. WO 2015/051043 A1. *Amgen Inc.* **2015**.
- (36) Proschak, E.; Heitel, P.; Kalinowsky, L.; Merk, D. Opportunities and Challenges for Fatty Acid Mimetics in Drug Discovery. *J. Med. Chem.* **2017**, *60* (13), 5235–5266.
- (37) Hopkins, A. L.; Keserü, G. M.; Leeson, P. D.; Rees, D. C.; Reynolds, C. H. The Role of Ligand Efficiency Metrics in Drug Discovery. *Nat. Rev. Drug Discov.* **2014**, *13* (2), 105–121.
- (38) Helmstädter, M.; Schierle, S.; Isigkeit, L.; Proschak, E.; Marschner, J. A.; Merk, D. Activity Screening of Fatty Acid Mimetic Drugs Identified Nuclear Receptor Agonists. *Int. J. Mol. Sci.* **2022**, *23* (17), 10070.
- (39) Brown, K.; Cavalla, J. F.; Green, D.; Wilson, A. B. Diaryloxazole and Diarylthiazolealkanoic Acids: Two Novel Series of Non-Steroidal Anti-Inflammatory Agents. *Nature* **1968**, *219* (5150), 164.
- (40) Nickel, J.; Gohlke, B. O.; Erehman, J.; Banerjee, P.; Rong, W. W.; Goede, A.; Dunkel, M.; Preissner, R. SuperPred: Update on Drug Classification and Target Prediction. *Nucleic Acids Res.* **2014**, *42* (W1), W26–W31.
- (41) Daina, A.; Michielin, O.; Zoete, V. SwissTargetPrediction: Updated Data and New Features for Efficient Prediction of Protein Targets of Small Molecules. *Nucleic Acids Res.* **2019**, *47* (W1), W357–W364.
- (42) Keiser, M. J.; Roth, B. L.; Armbruster, B. N.; Ernsberger, P.; Irwin, J. J.; Shoichet, B. K. Relating Protein Pharmacology by Ligand Chemistry. *Nat. Biotechnol.* **2007**, *25* (2), 197–206.
- (43) Daina, A.; Michielin, O.; Zoete, V. SwissADME: A Free Web Tool to Evaluate Pharmacokinetics, Drug-Likeness and Medicinal Chemistry Friendliness of Small Molecules. *Sci. Rep.* **2017**, *7*, 42717.
- (44) Daina, A.; Zoete, V. A BOILED-Egg To Predict Gastrointestinal Absorption and Brain Penetration of Small Molecules. *ChemMedChem* **2016**, *11* (11), 1117–1121.
- (45) Yuan, M.; Yang, H. Y.; Zhong, Y. H.; Zhuang, X. M.; Li, H. Assessment of Blood Brain Barrier Penetration of Drugs Using a Rat Steady-State Brain Distribution Model. *J. Int. Pharm. Res.* **2015**, *42* (5), 625–629.
- (46) Willems, S.; Merk, D. Medicinal Chemistry and Chemical Biology of Nurr1 Modulators: An Emerging Strategy in Neurodegeneration. *J. Med. Chem.* **2022**, *65* (14), 9548–9563.
- (47) Willems, S.; Marschner, J. A.; Kilu, W.; Faudone, G.; Busch, R.; Duensing-Kropp, S.; Heering, J.; Merk, D. Nurr1 Modulation Mediates Neuroprotective Effects of Statins. *Adv. Sci.* **2022**, *9* (18), 2104640.
- (48) Gao, L.; Zhou, W.; Symmes, B.; Freed, C. R. Re-Cloning the N27 Dopamine Cell Line to Improve a Cell Culture Model of Parkinson's Disease. *PLoS One* **2016**, *11* (8), e0160847.
- (49) Uhlén, M.; Fagerberg, L.; Hallström, B. M.; Lindskog, C.; Oksvold, P.; Mardinoglu, A.; Sivertsson, Å.; Kampf, C.; Sjöstedt, E.; Asplund, A.; Olsson, I. M.; Edlund, K.; Lundberg, E.; Navani, S.; Szigartyo, C. A. K.; Odeberg, J.; Djureinovic, D.; Takanen, J. O.; Hober, S. et al. Proteomics. Tissue-Based Map of the Human Proteome. *Science* (80-.). **2015**, *347* (6220), 1260419.
- (50) Kadkhodaei, B.; Ito, T.; Joodmardi, E.; Mattsson, B.; Rouillard, C.; Carta, M.; Muramatsu, S. I.; Sumi-Ichinose, C.; Nomura, T.; Metzger, D.; Chambon, P.; Lindqvist, E.; Larsson, N. G.; Olson, L.; Björklund, A.; Ichinose, H.; Perlmann, T. Nurr1 Is Required for Maintenance of Maturing and Adult Midbrain Dopamine Neurons. *J. Neurosci.* **2009**, *29* (50), 15923–15932.
- (51) Saucedo-Cardenas, O.; Quintana-Hau, J. D.; Le, W. D.; Smidt, M. P.; Cox, J. J.; De Mayo, F.; Burbach, J. P. H.; Conneely, O. M. Nurr1 Is Essential for the Induction of the Dopaminergic Phenotype and the Survival of Ventral Mesencephalic Late Dopaminergic Precursor Neurons. *Proc. Natl. Acad. Sci. U. S. A.* **1998**, *95* (7), 4013–4018.
- (52) Langer, T.; Wermuth, C. G. Selective Optimization of Side Activities (SOSA): A Promising Way for Drug Discovery. In *Polypharmacology in Drug Discovery*; John Wiley & Sons, Inc.: Hoboken, NJ, USA, 2012; pp 227–243.
- (53) Wermuth, C. G. Selective Optimization of Side Activities: Another Way for Drug Discovery. *J. Med. Chem.* **2004**, *47* (6), 1303–1314.
- (54) Pauli, G. F.; Chen, S.-N.; Simmler, C.; Lankin, D. C.; Gödecke, T.; Jaki, B. U.; Friesen, J. B.; McAlpine, J. B.; Napolitano, J. G. Importance of Purity Evaluation and the Potential of Quantitative ¹H NMR as a Purity Assay. *J. Med. Chem.* **2014**, *57* (22), 9220–9231.
- (55) Flesch, D.; Cheung, S.-Y.; Schmidt, J.; Gabler, M.; Heitel, P.; Kramer, J.; Kaiser, A.; Hartmann, M.; Lindner, M.; Lüddens-Dämgen, K.; Heering, J.; Lamers, C.; Lüddens, H.; Wurglics, M.; Proschak, E.; Schubert-Zsilavecz, M.; Merk, D. Nonacidic Farnesoid X Receptor Modulators. *J. Med. Chem.* **2017**, *60* (16), 7199–7205.
- (56) Gellrich, L.; Heitel, P.; Heering, J.; Kilu, W.; Pollinger, J.; Goebel, T.; Kahnt, A.; Arifi, S.; Pogoda, W.; Paulke, A.; Steinhilber, D.; Proschak, E.; Wurglics, M.; Schubert-Zsilavecz, M.; Chaikuad, A.; Knapp, S.; Bischoff, I.; Fürst, R.; Merk, D. L-Thyroxin and the Nonclassical Thyroid Hormone TETRAC Are Potent Activators of PPAR γ . *J. Med. Chem.* **2020**, *63* (13), 6727–6740.
- (57) Rau, O.; Wurglics, M.; Paulke, A.; Zitzkowski, J.; Meindl, N.; Bock, A.; Dingermann, T.; Abdel-Tawab, M.; Schubert-Zsilavecz, M. Carnosic Acid and Carnosol, Phenolic Diterpene Compounds of the Labiate Herbs Rosemary and Sage, Are Activators of the Human Peroxisome Proliferator-Activated Receptor Gamma. *Planta Med.* **2006**, *72* (10), 881–887.
- (58) Heitel, P.; Achenbach, J.; Moser, D.; Proschak, E.; Merk, D. DrugBank Screening Revealed Alitretinoin and Bexarotene as Liver X Receptor Modulators. *Bioorg. Med. Chem. Lett.* **2017**, *27* (5), 1193–1198.
- (59) Schmidt, J.; Klingler, F.-M.; Proschak, E.; Steinhilber, D.; Schubert-Zsilavecz, M.; Merk, D. NSAIDs Ibuprofen, Indometacin and Diclofenac Do Not Interact with Farnesoid X Receptor. *Sci. Rep.* **2015**, *5*, 14782.
- (60) Sadowski, I.; Ma, J.; Triezenberg, S.; Ptashne, M. GAL4-VP16 Is an Unusually Potent Transcriptional Activator. *Nature* **1988**, *335*, 563–564.
- (61) Budzyński, M. A.; Puustinen, M. C.; Joutsen, J.; Sistonen, L. Uncoupling Stress-Inducible Phosphorylation of Heat Shock Factor 1 from Its Activation. *Mol. Cell. Biol.* **2015**, *35* (14), 2530–2540.
- (62) Seuter, S.; Väisänen, S.; Rådmark, O.; Carlberg, C.; Steinhilber, D. Functional Characterization of Vitamin D Responding Regions in the Human 5-Lipoxygenase Gene. *Biochim. Biophys. Acta - Mol. Cell Biol. Lipids* **2007**, *1771* (7), 864–872.
- (63) Sugano, K.; Hamada, H.; Machida, M.; Ushio, H. High Throughput Prediction of Oral Absorption: Improvement of the Composition of the Lipid Solution Used in Parallel Artificial Membrane Permeation Assay. *SLAS Discov.* **2001**, *6* (3), 189–196.